NEUROSCIENCE

The impact of hUC MSC–derived exosome-nanoliposome hybrids on α-synuclein fibrillation and neurotoxicity

Farhang Aliakbari[1,2]*, Kimia Marzookian[1], Soha Parsafar[1], Hamdam Hourfar[1], Zahra Nayeri[1], Arghavan Fattahi[1], Mohammad Raeiji[1], Narges Nasrollahi Boroujeni[1,3], Daniel E. Otzen[4], Dina Morshedi[1]*

Amyloid aggregation of α-synuclein (αSN) protein amplifies the pathogenesis of neurodegenerative diseases (NDs) such as Parkinson's disease (PD). Consequently, blocking aggregation or redirecting self-assembly to less toxic aggregates could be therapeutic. Here, we improve brain-specific nanocarriers using a hybrid of exosomes (Ex) from human umbilical cord mesenchymal stem cells (hUC MSCs) and nanoliposomes containing baicalein (Ex-NLP–Ba) and oleuropein (Ex-NLP–Ole). The hybrids contained both lipid membranes, Ex proteins, and baicalein or oleuropein. Fluorescence resonance energy transfer analysis confirmed their proper integration. The hybrids reduced the extent of αSN fibrillation and interfered with secondary nucleation and disaggregation. They not only reduced αSN pathogenicity but also enhanced drug internalization into cells, surpassing the efficacy of NLP alone, and also crossed the blood-brain barrier in a cellular model. We conclude that Ex can be successfully extracted and efficiently merged with NLPs while retaining its original properties, demonstrating great potential as a theranostic drug delivery vehicle against NDs like PD.

INTRODUCTION

Neurodegenerative diseases (NDs) are pleiotropic illnesses that involve many factors and effects, resulting in complicated pathologies. Hence, multifaceted treatments will likely be necessary for effective therapy. One of the primary concerns is neuronal damage, which serves as a marker for the progression of the disease. In addition, two other factors that play a substantial role in NDs are inflammation and compensation for damaged cells (neuroprotection/neurodegeneration). It is widely accepted that one of the main causes of Parkinson's disease (PD) and related diseases (collectively called synucleinopathies) is the accumulation of aggregates of the protein α-synuclein (αSN) (*1*, *2*). These manifest intracellularly as large plaque-like structures known as Lewy bodies in affected cells. αSN aggregates can be transmitted to neighboring cells (*3*) and thus spread to a large area of the brain, accompanied by profound damage (*4*). Currently, treatment for PD is palliative and focuses on pain relief, analgesia, or compensating for dopamine depletion. Curative therapies, e.g., eliminating toxic proteins and/or regenerating damaged cells, are still in the preclinical stages (*5*). One important challenge in developing therapeutic strategies for αSN is the formation of intracellular plaques. That is, potent molecules that can inhibit αSN fibrillation must be delivered into neurons (*5*–*8*). Numerous small molecules can hinder fibrillation, reducing the formation of toxic aggregates and subsequent neurodegeneration (*5*, *9*–*13*). However, the clinical application of these molecules is challenging due to their hydrophobic nature and limited stability. To overcome this, liposomal nanosystems have been used (*14*, *15*). We have previously shown that the hydrophobic small molecules baicalein and oleuropein inhibit αSN fibrillation (*7*, *16*). We have also shown that zwitterionic nanoliposomes (NLPs) stabilize baicalein and maintain its antioxidant and neuroprotective activity over time, also reducing αSN fibrillation and subsequent cell death (*7*, *17*). This demonstrated the use of NLPs as carriers for hydrophobic and chemically unstable drugs to treat αSN aggregates. Nevertheless, although the NLPs were able to cross the blood-brain barrier (BBB), there is still room for further improvement.

Mesenchymal stem cells (MSCs) are multipotent stem cells that have the unique ability of self-renewal and differentiation (*18*). MSCs have two distinct therapeutic properties, namely, multipotentiality (the ability to differentiate into different types of cells) and the secretion of active compounds, which may be contained in extracellular vehicles such as exosomes (Ex) (*19*, *20*). In recent years, the use of MSCs for tissue repair has expanded in regenerative medicine (*21*) and the benefits of their transplantation are not only based on direct differentiation to target cells but also based on their capacity to secrete biologically active compounds such as Ex. These compounds are essential in restoring the microenvironment and promoting the regenerative process (*22*–*24*).

Ex are derived from endosomes containing various macromolecules including noncoding RNAs, proteins, and lipids that are involved in regulating the differentiation, activity, division, and function of recipient cells (*25*, *26*). Ex contribute to the clearance of cells from macromolecules as well as the transfer of macromolecules from cell to cell (*27*–*29*). Ex mediate their activity over long distances by transporting RNA and proteins to recipient cells (*30*). Ex content reflects their tissue origin (*31*). Accordingly, Ex are promising candidates for tissue regeneration, and their contents may halt the progression of some diseases. MSC-derived Ex have major antiapoptotic and anti-inflammatory effects and lead to angiogenic

[1]Bioprocess Engineering Department, Institute of Industrial and Environmental Biotechnology, National Institute of Genetic Engineering and Biotechnology, Tehran, Iran. [2]Molecular Medicine Group, Robarts Research Institute, Schulich School of Medicine and Dentistry, University of Western Ontario, London, ON, Canada. [3]Department of Biomedicine and Prevention, University of Rome Tor Vergata, Rome, Italy. [4]Interdisciplinary Nanoscience Centre (iNANO) and Department of Molecular Biology and Genetics, Aarhus University, Gustav Wieds Vej 14, DK-8000 Aarhus C, Denmark.
*Corresponding author. Email: morshedi@nigeb.ac.ir (D.M.); aliakbari@nigeb.ac.ir (F.A.)

stimulation, regeneration, and improvement of cell function in different treated tissues (*24*, *32*–*36*). However, MSC-derived Ex need to cross the BBB to reach damaged neurons. Ex may be trapped in nonspecific organs, especially in the lungs and liver, leading to their failure to reach the original target (*32*). Ex are naturally occurring carriers of macromolecules in the body, making their transport system a promising tool for medical applications. However, the efficient and reproducible loading of drugs into Ex, as well as their scalable extraction, remains a challenge, limiting their potential as drug carriers. One effective strategy to overcome this limitation is to combine Ex with other carriers, specifically liposomes, which have more structural similarities. Combining Ex and liposomes enhances their therapeutic potential (*37*) and overcomes limitations inherent in each cargo system [e.g., inadequate effectiveness in encapsulating big nucleic acids in Ex or resistance to transfection by liposomes alone (*38*)].

Here, we develop Ex-NLP hybrids derived from human umbilical cord MSCs (hUC MSCs) and loaded with baicalein or oleuropein to assess their ability to inhibit αSN fibrillation and pass through the BBB model. To make these changes, we deliberately chose zwitterionic NLPs over cationic or anionic counterparts due to their unique advantages for treating αSN aggregation and PD. Unlike cationic liposomes, which may be toxic (*39*), and anionic liposomes, which may induce fibrillation by altering protein conformation (*40*, *41*), zwitterionic NLPs exhibit biocompatibility, the ability to encapsulate various molecules, and low immunogenicity and toxicity (*14*, *42*). In addition, zwitterionic NLPs exhibit prolonged circulating half-lives compared to their cationic or anionic counterparts (*43*). Moreover, our previous studies have demonstrated their effectiveness in affecting αSN fibrillation and neurotoxicity (*17*). We also incorporated MSC-derived Ex into the hybrid composition due to their regenerative and immunomodulatory properties, which offer notable potential in the treatment of NDs. Therefore, such Ex may contribute to neuronal repair, reduce neuroinflammation, and carry a bioactive cargo that enhances neuroprotection. As natural carriers, they facilitate intercellular communication and have the ability to traverse the BBB, a critical factor for ensuring effective drug delivery to the brain (*44*). Thus, MSC-derived Ex may play a pivotal role in augmenting the overall efficacy of the hybrid system for ND therapy.

Effective drug delivery to the brain is crucial, and the use of appropriate nanocarriers plays an important role in this process. The study presents a multifaceted approach to treating amyloid-related disorders, showing that anti-amyloid drugs delivered by NLP in combination with MSC-derived Ex may help to protect vulnerable neurons by preventing and reversing amyloid formation, aided by the MSCs' ability to increase drugs internalization into the cells and cross the BBB.

RESULTS

hUC MSCs isolation and characterization

MSCs were first isolated from hUC using modified-explant culture using metal mesh grids (fig. S1), and then characterized using flow cytometry based on their specific markers. CD34, CD45, and HLA-DR markers, which are associated with common impurities in stem cell cultures, were negative, while CD73, CD44, and CD29 markers, which are specific to MSCs, were positive (fig. S2).

hUC MSC–derived exosome purification from suitable conditioned media

Manipulating the culture media conditions has a direct effect on the characteristics and contents of MSCs secretome. Therefore, as described in our recent study and summarized in Fig. 1, hUC MSCs were cultured in the serum-free media of RPMI 1640 and Dulbecco's modified Eagle's medium (DMEM) high glucose [80:20 (v/v)] to produce and purify Ex. Ex were then isolated by collecting the conditioned media after 48 hours, purified by Exo-spin kit, quantified using a BCA kit, and protein concentration was adjusted to 400 μg/ml. Transmission electron microscopy (TEM) images demonstrated that the purified hUC MSC–derived Ex were spherical and unilamellar with an average diameter of 48.32 ± 23.44 nm. Dynamic light scattering (DLS) specified an average particle size of diameter 90.57 ± 3.21 nm based on the number [polydispersity index (PdI) = 0.193 ± 0.0098]. Western blot analysis indicated the presence of two exosomal markers, CD29 and Alix (Fig. 1).

Fabrication of hybrids of hUC MSC–derived exosomes and NLP

The liposomal nanosystems consisting of neutral phospholipid (DPPC, 1,2-dipalmitoyl-*sn*-glycero-3-phosphocholine), 1,2-dipalmitoyl-sn-glycero-3-phosphoethanolamine-N-[methoxy(polyethylene glycol)-2000] (PEG2000 PE), and cholesterol-containing anti-neurotoxin small molecules baicalein or oleuropein were formulated. The ratio of baicalein to DPPC was 1:3 (mol/mol), while the optimized ratio for oleuropein to DPPC was 1:4 (mol/mol).

Ex and NLPs were fused in several cycles of the freezing-thawing procedure (Fig. 2A). Förster resonance energy transfer (FRET) (described in the Supplementary Materials) was used to assess the fusion efficacy of Ex-NLP (*45*, *46*) using the two fluorescent dyes, fluorescein isothiocyanate (FITC), and Rhodamine B (RB). After exciting the FITC molecules, two emission peaks were determined, related to FITC and RB. After integrating the Ex and NLP, the fluorescence intensity of FITC increased, while the fluorescence intensity for RB decreased as the number of cycles increased (Fig. 2B). The reduction in FRET effect was attributed to the increase in the distance between FITC and RB molecules due to dilution through fusion with Ex. Assessing the extent of fusion between Ex and NLP poses challenges due to the lack of a definitive benchmark for complete fusion. Fusion is a dynamic process influenced by various factors, making it challenging to establish a universal standard for completeness. While we cannot quantify the extent of fusion directly, the decline in signal observed in our study serves as robust evidence for a degree of interaction between Ex and NLP, reflecting changes in the nanosystem's composition. The success of drug delivery across barriers is intricately linked to the extent of fusion, as a more extensive fusion may enhance the payload's release and interaction with target cells. The degree of fusion can influence the stability and functionality of the nanosystem, affecting its therapeutic efficacy.

Fourier transform infrared (FTIR) was also used to confirm the integration of Ex and NLP incorporating the small molecules. Figure S3 shows the FTIR spectra of Ex-NLP–Ba (fig. S3A), Ex-NLP–Ole (fig. S3B), pure baicalein (fig. S3C), pure oleuropein (fig. S3D), and pure Ex (fig. S3E). In the FTIR spectra of pure baicalein, the band at 3408 cm^{-1} reports on O─H stretching, and 1617 cm^{-1} is for aromatic structures. Incorporated baicalein in Ex-NLP led to a broad and intense peak around 3415 cm^{-1}

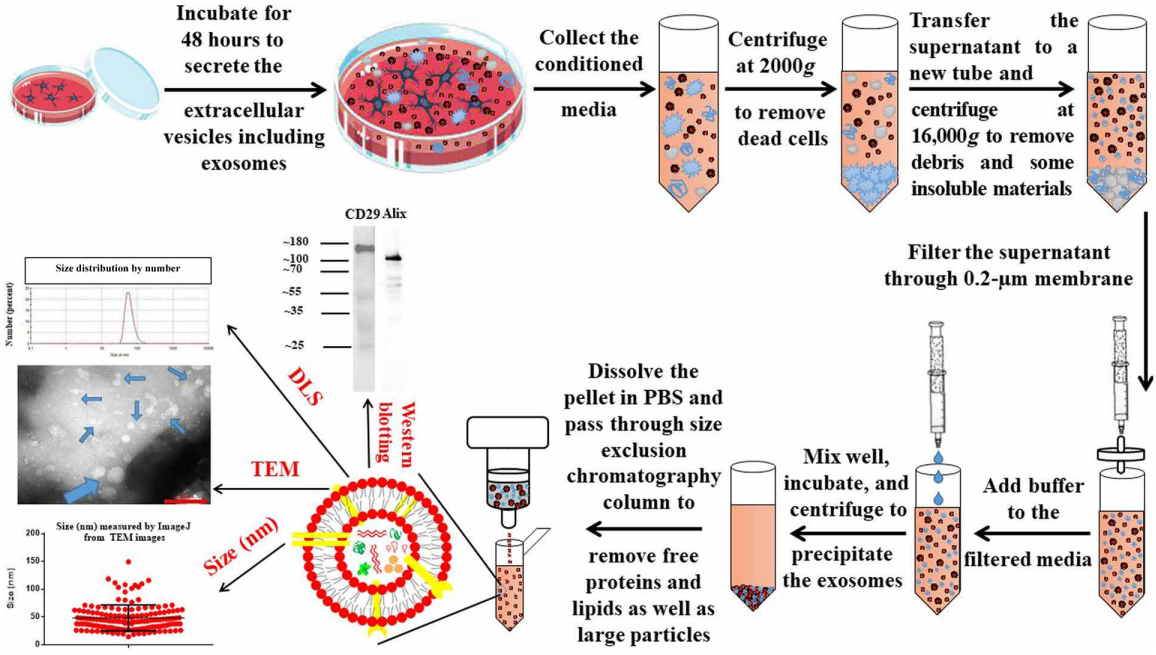

Fig. 1. Schematic diagrams of the extraction and purification steps of hUC MSC–derived Ex and its characterization. After isolating the hUC MSCs using mesh-covered plates, and expanding them, the Ex were extracted and purified using precipitation and size exclusion chromatography methods. Components in the extracted Ex were determined by Western blot, while size was measured using DLS and TEM images using ImageJ. Scale bar, 150 nm. PBS, phosphate-buffered saline.

which relates to stretching of both OH and NH present in Ex-NLP–Ba, either unbound or hydrogen bonded. On the other hand, Ex and NLP have water molecules in their vesicles which increase the intensity of this peak. The peak at 1637 cm^{-1} present in Ex, Ex-NLP, and Ex-NLP–Ba is mostly related to C═O stretching in peptide bonds. Another peak around 2900 cm^{-1} is related to acyl groups, which is strong in all complexes containing liposomes. The peak around 1110 cm^{-1}, present in Ex, Ex-NLP, and Ex-NLP–Ba could refer to C—N stretching related to proteins in Ex. Regarding the other hybrid (Ex-NLP–Ole), the FTIR spectrum of oleuropein showed distinct peaks at 3400 cm^{-1} (for O—H stretching), 1632 cm^{-1} (for C═C stretching), and 1076 cm^{-1} (for C—O stretching in ester groups or secondary alcohol). The 3400-cm^{-1} peak is wider and stronger in oleuropein because there are more OH groups in this small molecule compared to baicalein. Both Ex and Ex-NLP–Ole spectra displayed uniform peaks (double peaks) at 1637 and 1617 cm^{-1} (amide bonds and aromatic structures), which are similar to the Ex-NLP–Ba spectrum. This suggests that Ex-NLP can be identified with small molecules through this feature, as it remains unchanged in both formulations. To further support the fusion, SDS–polyacrylamide gel electrophoresis (SDS-PAGE) analysis showed the same pattern of protein for Ex, Ex-NLP–Ba, and Ex-NLP–Ole (fig. S3F).

We also evaluated fluorescence intensity after the fusion of drug-containing NLP with Ex. The near-ultraviolet fluorescence intensity increased significantly for the Ex-NLP–Ole hybrid, which we attribute to the presence of intrinsic fluorophores (Trp and Tyr residues) in the proteins of the Ex (Fig. 2C). The chemical and physical properties of DPPC, oleuropein, and baicalein, which were extracted from PubChem, are presented in table S1. This table indicates that oleuropein has a negative Xlog*P* value and a more complex and flexible chemical structure than baicalein. It appears that in the presence of oleuropein, different interactions occur that lead to an enhanced fluorescence intensity in Ex-NLP–Ole.

Accordingly, the surfaces of the two membranes were well hybridized and the structure of the nanosystem was still preserved. In addition, the exosomal proteins and the cargo molecules baicalein and oleuropein remained on the hybrid.

Through disturbing αSN fibrillation, Ex-NLP–Ba and Ex-NLP–Ole affect the final products

Previous studies have shown that baicalein and oleuropein are potent inhibitors against αSN fibrillation and toxicity (*7*, *16*, *47*); however, their curative efficiency is lost in biological systems. To investigate the effect of Ex-NLP–Ba and Ex-NLP–Ole on αSN fibrillation, 20 and 100 μM of each hybrid [based on baicalein or oleuropein concentrations at three different ratios of 1:10, 1:20, and 1:100 (w/w) of Ex:NLP] were incubated with 70 μM of αSN monomers, and the kinetics of fibrillation were obtained during 48 hours (Fig. 3, A, C, and E). Both hybrids reduced the endpoint fluorescence level in a concentration-dependent manner (Fig. 3, B, D, and F). We interpret this to mean that the hybrids reduce the extent of fibrillation more than those of nucleation phase or growth rate. The total percentage of thioflavin T (ThT) signal reduction by hybrids during the fibrillation process was approximately between 42 and 60%, 45 and 75%, and 40 and 77% for the hybrids at the ratios of 1:10, 1:20, and 1:100 (w/w) of Ex:NLP, respectively. Purified Ex themselves had an impact on αSN fibrillation with the total percentage of ThT signal reduction of 32 to 43% for Ex (20 to 200 μg/ml; fig. S4, A to E).

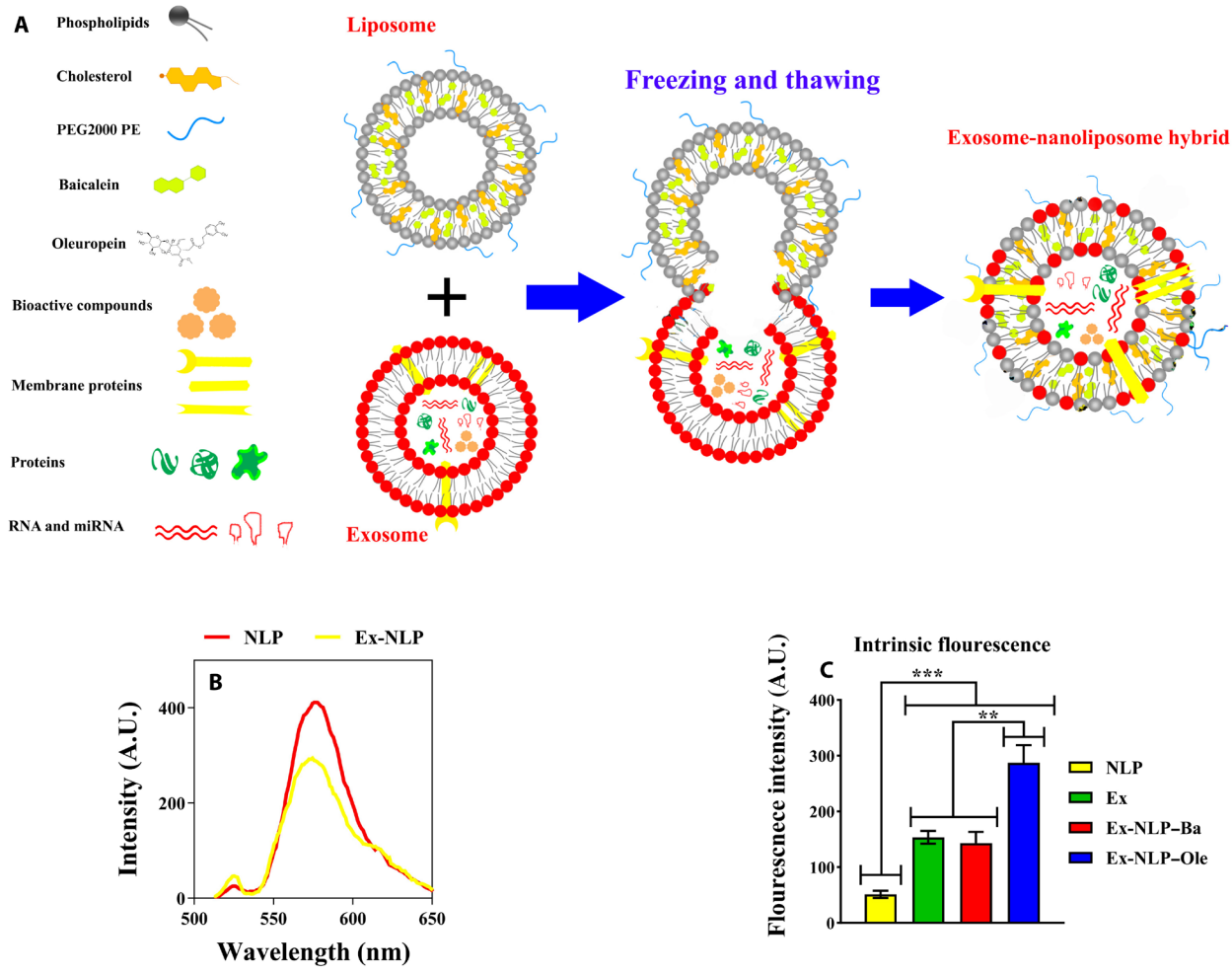

Fig. 2. Formulation of Ex-NLP hybrid containing baicalein or oleuropein. (**A**) The schematic diagram illustrates the integration of the extracted Ex and NLP and the mixing of their contents. Ten cycles of freezing and thawing in liquid nitrogen and room temperature were used. miRNA, microRNA. (**B**) Fluorescence resonance energy transfer technique to evaluate the fusion. The fluorescence spectrum with the excitation at 495 nm (FITC, fluorescein isothiocyanate) and emissions at 525 nm (FITC) and 570 nm (RB) at cycle five. A.U., arbitrary units. With increasing the number of freezing and thawing cycles, the emission of fluorescence intensity of FITC increases, while that of RB decreases, which indicates dilution of RB and thus successful integration of Ex and NLP. (**C**) Intrinsic tryptophan fluorescence intensity of NLP before and after fusion with Ex in the presence of baicalein or oleuropein. The excitation and emission were set at 280 and 310 nm, respectively ($N = 3$, mean ± SD, $^{**}P \leq 0.01$, $^{***}P \leq 0.001$).

In silico evidence that αSN may interact with Ex-NLP–Ba and Ex-NLP–Ole during fibrillation

Our previous results suggest that αSN may interact with Ex-NLP hybrids containing small molecules, reducing fibrillation. Therefore, in silico procedures were used to investigate possible interactions. The interaction may occur through the binding of αSN to Ex (for instance, via exosomal proteins), to the lipid membrane of hybrids, or to baicalein and oleuropein. The interactions of αSN with neutrally charged lipid membrane and baicalein have already been studied extensively (*7*, *17*, *47*, *48*). Oleuropein could also interact with αSN as well (*16*, *49*, *50*). Consequently, the interactions between αSN and specific Ex proteins were investigated in silico. Ex proteins include (i) general markers of Ex: tetraspanins (CD81 and CD9), (ii) proteins associated with the multivesicular body (Alix and TSG101); (iii) specific Ex markers of MSCs (CD44 and CD73), and (iv) other markers (CD29, syntenin-1, and syntenin-4). Table S2 summarizes the information on the selected proteins. Protein-protein binding analysis was performed for three αSN structures (monomer, 5-chain aggregates, and 10-chain aggregates as detailed in Materials and Methods) and exosomal markers with HDOCK server. For each simulation, the best docking scores of the prediction models out of 100 models obtained from HDOCK are shown in Fig. 4A. We observed that αSN species of 10-chain aggregates represented the lowest docking score (i.e., strongest binding affinity) with CD81, CD9, Alix, CD44, CD73, syntenin-1, and syntenin-4 followed by 5-chain aggregates, and monomers. In addition, 10-chain αSN aggregates had lower binding energies for TSG101 and CD29 than αSN monomers (Fig. 4A). The model with the best docking score for 10-chain aggregates and each protein marker was shown in Fig. 4B. Overall, these results indicate that in the aggregation processes of αSN, with increasing αSN chains in aggregated species, its tendency to bind to Ex protein markers was also increased. As a result, binding such

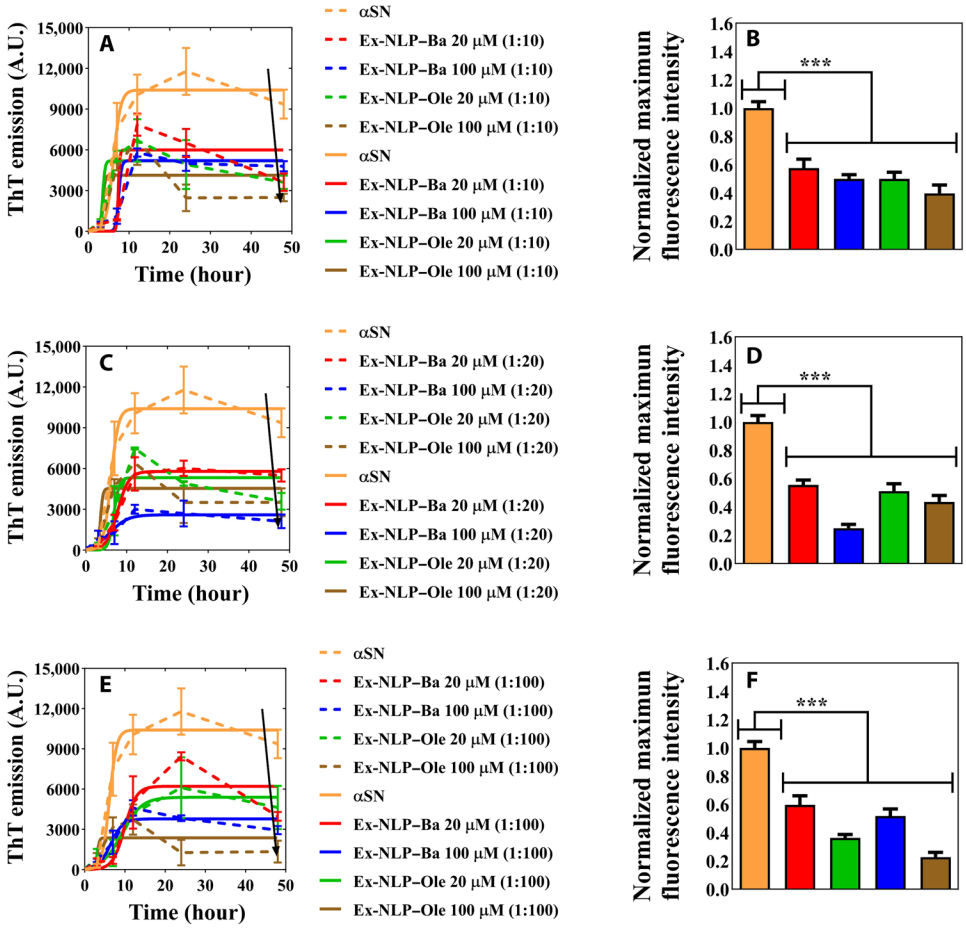

Fig. 3. The effect of the Ex-NLP–Ba and Ex-NLP–Ole on αSN fibrillation. ThT signals (**A**, **C**, and **E**) and normalized maximum ThT emission (**B**, **D**, and **F**) derived from 70 μM αSN incubated with or without Ex-NLP–Ba or Ex-NLP–Ole (20 and 100 μM, based on baicalein or oleuropein concentrations) at 37°C throughout 48 hours. Ex-NLP–Ba or Ex-NLP–Ole were formulated at the ratio of 1:10 (w/w of Ex:NLP) [(A) and (B)], 1:20 [(C) and (D)], and 1:100 [(E) and (F)]. Arrows indicate a reduction in the final product due to the effect of Ex-NLP–Ba or Ex-NLP–Ole. Dashed lines: ThT signals taken from fluorimetry; continuous lines: regression or trend lines (fitted curve). $N = 3$, mean ± SD, $^{***}P \leq 0.001$.

aggregates to the Ex can prevent the aggregation from advancing to the fibril or forming toxic aggregates. Nevertheless, it is worth mentioning that while computational models provide valuable insights into complex biological interactions, they inherently oversimplify the complex and dynamic nature of biological systems. For example, protein-protein docking studies do not fully capture the range of interactions and behaviors present in biological systems, such as the simultaneous impact of all proteins on the binding of each protein to αSN. Nevertheless, the credibility of our computational models was enhanced by their consistency with our experimental results, where the Ex or hybrid of Ex-NLP seems to target the endpoint product rather than the early stages of fibrillation.

Ex-NLP–Ba and Ex-NLP–Ole affect secondary nucleation and depolymerize αSN mature fibrils

Secondary nucleation is a critical stage in the fibrillation process that can lead to the formation of a new series of toxic aggregates. To bypass primary nucleation (formation of fibrillation nuclei) and focus on the impact of Ex-NLP–Ba/Ole hybrids on secondary processes, we add sonicated mature fibrils as seeds (fig. S5). αSN monomers were then added in the presence or absence of Ex-NLP–Ba or Ex-NLP–Ole and the kinetics of fibrillation were then monitored for 48 hours. Ex-NLP–Ba and Ex-NLP–Ole at concentrations of 20 and 100 μM and with three different ratios of Ex-NLP including 1:10 (Fig. 5, A and B), 1:20 (Fig. 5, C and D), and 1:100 (Fig. 5, E and F) were observed to effectively interfere with secondary nucleation, leading to inhibition of the fibrillation process (Fig. 5, A, C, and E) and reduction in the extent of fibrillation (Fig. 5, B, D, and F). The total percentage of ThT signal reduction mediated by hybrids during the secondary nucleation process was approximately between 55 and 78%, 72 and 75%, and 73 and 75% for the hybrids at the ratios of 1:10, 1:20, and 1:100 (w/w) of Ex:NLP, respectively. Ex themselves affect secondary nucleation, but not as well as the hybrids (fig. S6, A and B), suggesting an enhanced effect of the hybrids. These findings, along with the results obtained from primary fibrillation kinetics (Fig. 3), suggest an interaction between the drug-containing Ex-NLP hybrids and the αSN aggregates. This interaction may occur via the phospholipid membrane, the Ex surface proteins, or the small molecules they carry.

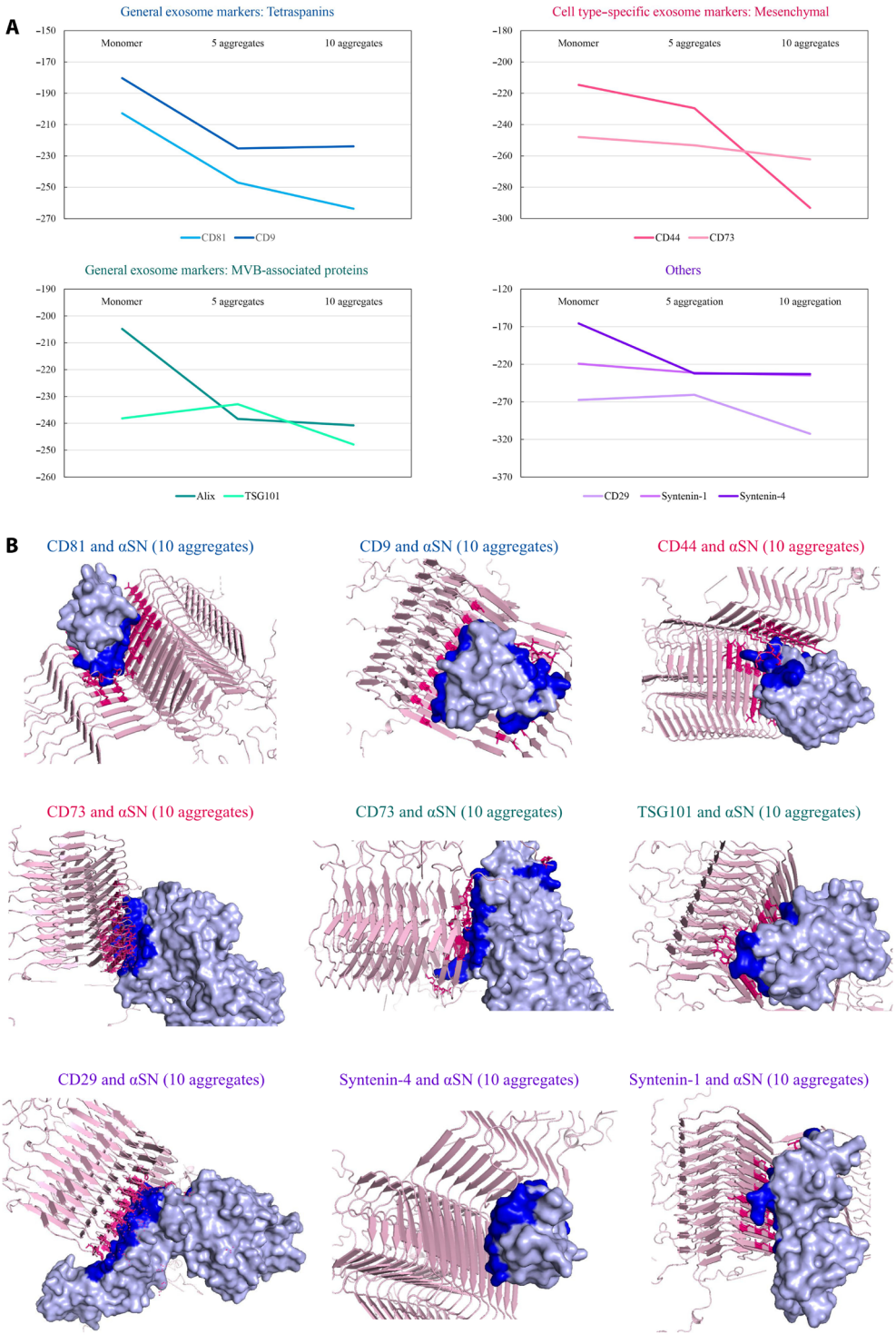

Fig. 4. In silico study to assess the interaction of αSN with exosomal proteins. The interaction of αSN with specific exosomal proteins including CD81 [Protein Data Bank (PDB) ID: 5 M33] and CD9 (PDB ID: 6Z1V); CD44 (PDB ID: 1UUH) and CD73 (PDB ID: 6TVE); Alix (PDB ID: 5WA1) and TSG101 (PDB ID: 3OBQ); and CD29 (PDB ID: 4WK0), syntenin-1 (PDB ID: 1W9E), and syntenin-4 (PDB ID: 1OBY) was investigated. (**A**) The protein-protein docking score rates for three different forms of αSN and the specific exosomal proteins. The *x* axis represents the three forms of αSN (monomers, 5-chain aggregates, and 10-chain aggregates), and the *y* axis shows the HDOCK docking scores. (**B**) Protein-protein HDOCK docking simulation results for 10 aggregates αSN (PDB ID:2N0A) and each exosome marker.

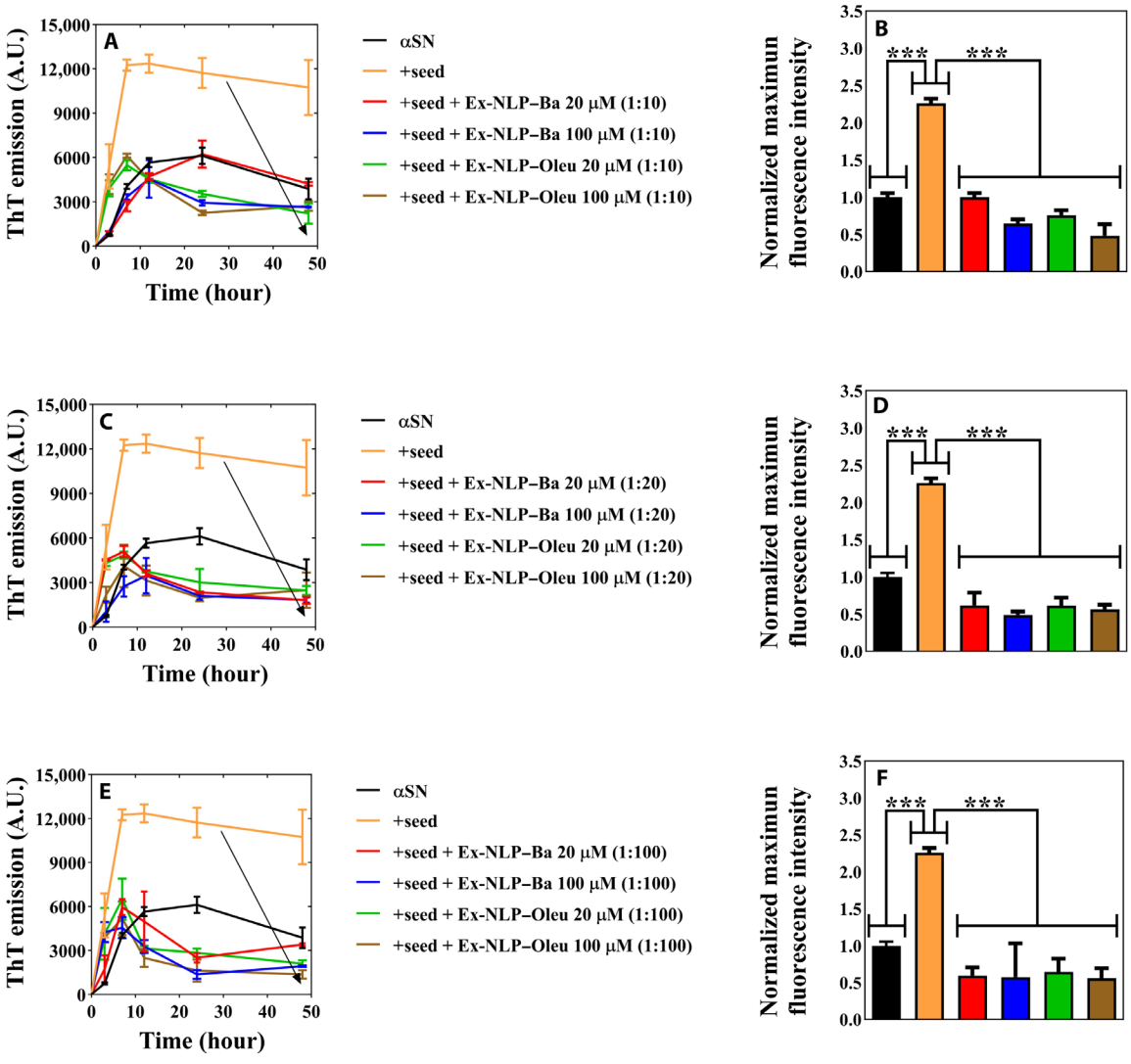

Fig. 5. The effect of Ex-NLP hybrid containing baicalein or oleuropein, both anti-neurotoxin drugs, on secondary nucleation of αSN. (**A**, **C**, and **E**) The kinetics of secondary fibrillation were observed for ratios of Ex:NLP hybrid [1:10, 1:20, and 1:100 (w/w)]. (**B**, **D**, and **F**) The normalized endpoint product was determined for each ratio. In addition, the arrows indicate a reduction in the final product, which can be attributed to the effect of Ex-NLP–Ba or Ex-NLP–Ole. $N = 3$, mean ± SD, $^{***}P \leq 0.001$.

Our next step was to evaluate whether Ex-NLP hybrids containing baicalein/oleuropein can successfully disaggregate/depolymerize mature αSN fibrils. We added Ex-NLP–Ba or Ex-NLP–Ole hybrids at specified ratios (at concentrations of 20 and 100 μM) to αSN fibrils (35 μM) and monitored ThT signals for 48 hours. Unlike Ex alone (fig. S6, C and D), all hybrids rapidly depolymerized αSN fibrils, converting them into smaller species (Fig. 6, A to F). The total percentage of reduction in the ThT signal mediated by hybrids during the disaggregation process was approximately between 47 and 56%, 49 and 61%, and 36 and 52% for the hybrids at the ratios of 1:10, 1:20, and 1:100 (w/w) of Ex:NLP, respectively. This is likely due to baicalein's or oleuropein's antifibrillary potential to interact and disaggregate αSN fibrils. As free Ex did not display any depolymerizing effect on the mature αSN fibrils (fig. S6, C and D), and given the fact that free-drug NLPs have the same lack of effect (*17*), we conclude that the observed disaggregation effect reflects the action of baicalein/oleuropein. To support this notion, we conducted in silico experiments to visualize the potential interaction of baicalein or oleuropein with aggregated forms of αSN. Specifically, we aimed to illustrate the interaction pattern of baicalein and oleuropein with αSN fibrils [Protein Data Bank (PDB) ID: 2N0A; Fig. 6G]. We conducted molecular docking simulations, which revealed that oleuropein exhibited a binding affinity of −8.3 kcal/mol with αSN fibrils (Fig. 6H). By comparison, baicalein's binding affinity was −7.1 kcal/mol (Fig. 6I). In addition, our findings indicated that amino acids 53 to 74 played a role in the interaction of both small molecules with αSN (Fig. 6, H and I). Previous studies have shown that these amino acids, as part of αSN's NAC (non–amyloid β component) region, are involved in the conversion of αSN to β sheet–rich structures (*51*–*53*).

The findings from the primary and secondary nucleation experiments, as well as depolymerization studies conducted in this investigation, collectively demonstrate that αSN exhibits interactions with hybrids containing small molecules during the fibrillation

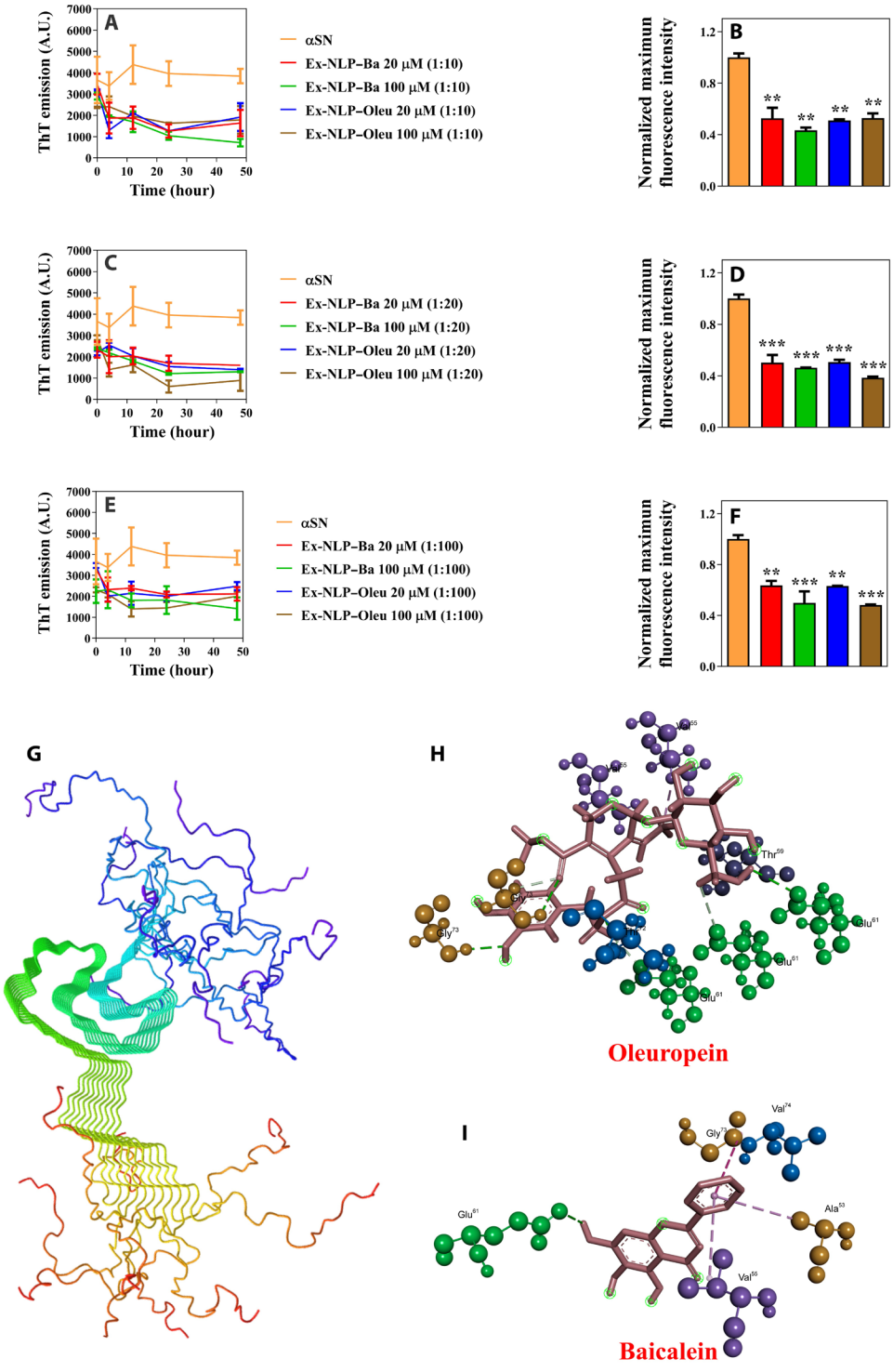

Fig. 6. The impact of baicalein/oleuropein-loaded Ex-NLP hybrids on the depolymerization of αSN fibers. (**A**, **C**, and **E**) ThT signals were measured during 48 hours while incubating αSN fibrils (35 μM) with 20 and 100 μM Ex-NLP–Ba or Ex-NLP–Ole at three ratios of 1:10, 1:20, and 1:100 of Ex:NLP. (**B**, **D**, and **F**) Normalized endpoint product after 48 hours derived from mature fibrils treated with Exo-NLP-Ba or Exo-NLP-Ole at 20 or 100 μM compared to that of control. (**G** to **I**) Docking simulation results for the interaction of oleuropein and baicalein with αSN fibrils. (G) The structure of αSN fibrils (2N0A) and illustration of its interactions with (H) oleuropein and (I) baicalein.

process. These interactions lead to a reduction in fibrillation and may consequently result in the production of less toxic compounds. Such interactions can occur through binding to exosomal proteins, lipid membranes, baicalein, or oleuropein. As for depolymerization, the presence of baicalein or oleuropein may cause them to adhere to the aggregates and break them apart.

Ex-NLP–Ba and Ex-NLP–Ole moderate the neurotoxicity of αSN

Aggregated species of αSN have been reported to cause neurodegeneration (*54*, *55*). Therefore, we assessed the performance of Ex-NLP–Ba and Ex-NLP–Ole in a cellular context. Mitochondrial metabolism of living cells using the 3-(4,5-dimethylthiazol-2-yl)-2,5-diphenyltetrazolium bromide (MTT) assay was tested on SHSY5Y cells treated with 10% (v/v) of 24-hour–aggregated species of αSN (70 μM) in the presence or the absence of Ex-NLP–Ba or Ex-NLP–Ole. In addition, the effect of these hybrids on the level of reactive oxygen species (ROS) and nitric oxide (NO) was evaluated. Neither hUC MSC–derived Ex (fig. S7A) nor the Ex-NLP–Ba and Ex-NLP–Ole (fig. S7B) showed significant neurotoxicity on SHSY5Y cells as shown in fig. S7. Moreover, the neurotoxicity of preincubated αSN in the presence of Ex-NLP–Ba or Ex-NLP–Ole was reduced compared to the control (as shown in Fig. 7A). In addition, the study found that the amount of intracellular ROS was decreased after treatment with preincubated αSN in the presence of either Ex-NLP–Ba or Ex-NLP–Ole, compared to preincubated αSN alone (Fig. 7B). Furthermore, the presence of αSN aggregates alone resulted in an increase in the amount of NO production, while treatment with aggregates formed in the presence of Ex-NLP–Ba or Ex-NLP–Ole resulted in a decreased amount of NO in the cells (Fig. 7C).

Ex-NLP–Ba and Ex-NLP–Ole are biocompatible and have antioxidant properties

A hemolysis assay using a blood agar medium was performed to assess the biocompatibility of Ex-NLP hybrids containing baicalein or oleuropein. We detected no hemolysis occurred when the blood agar media were treated with Ex-NLP–Ba and Ex-NLP–Ole, whereas complete hemolysis resulted from the control sample treated with bacteria (fig. S8A).

We then assessed the antioxidant activity of Ex-NLP–Ba and Ex-NLP–Ole using DPPH•. Ex alone does not have any antioxidant activity to scavenge the free radicals; however, Ex-NLP–Ba and Ex-NLP–Ole showed significant antioxidant activity (fig. S8, B and C).

Ex-NLP hybrids are capable of internalizing drugs into the cells more than NLP

Baicalein/oleuropein loaded onto Ex-NLP hybrids were taken up by SHSY5Y cells, highlighting the hybrid's ability to deliver drugs into

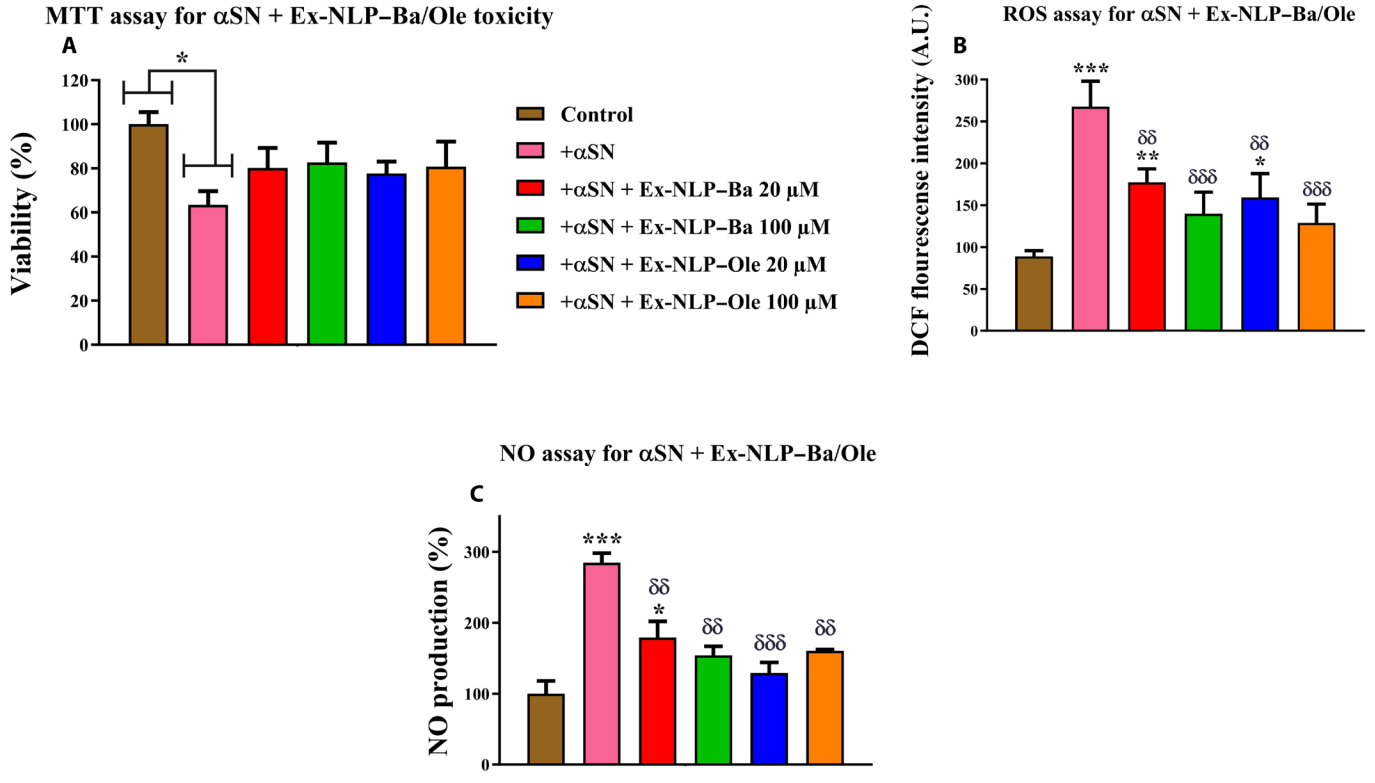

Fig. 7. Neurotoxicity of 24hour–aggregated species of αSN preformed in the presence or the absence of Ex-NLP hybrids containing baicalein or oleuropein (1:20 molar ratio with two concentrations of 20 and 100 μM based on baicalein or oleuropein) on SHSY5Y cells. (**A**) Assessment of cell viability using MTT assay, (**B**) intracellular level of ROS, and (**C**) intracellular NO production. * indicates significant differences between untreated cells and those treated with preincubated αSN (24 hours) in the presence of Ex-NLP–Ba and Ex-NLP–Ole, and δ indicates significant differences between treated cells with preincubated αSN (24 hours) alone and those treated with preincubated αSN in the presence of Ex-NLP–Ba and Ex-NLP–Ole ($N = 3$, means ± SD, $^{*}P \leq 0.05$, $^{\delta\delta}$, $^{**}P \leq 0.01$, and $^{\delta\delta\delta}$, $^{***}P \leq 0.001$).

cells. Ex-NLP hybrids at the ratio of 1:20 of Ex:NLP, at a concentration of 100 μM (based on small molecules), were added to the cells, out of which approximately 45 and 48% of baicalein and oleuropein, respectively, were taken up by the cells (Fig. 8, A and B). The comparable drug internalization percentages observed for baicalein and oleuropein in Fig. 8 align with their structural similarities as polyphenolic compounds and the consistent delivery platform provided by Ex:NLP. This result suggests a harmonized behavior in terms of cellular uptake for both compounds within the hybrid nanosystem. Furthermore, the Ex-NLP hybrids internalized a higher quantity of drugs into the cells within a specific time frame compared to NLP alone (Fig. 8, C and D). Ex-NLP–Ba and NLP-Ba as well as Ex-NLP–Ole and NLP-Ole were added to the SHSY5Y cells (ratio of 1:20 for Ex-NLP hybrids at a concentration of 100 μM for baicalein and oleuropein), and after 4 hours, the amount of internalized baicalein or oleuropein into the cells mediated by Ex-NLP or NLP was measured. The uptake rate of baicalein mediated by Ex-NLP was approximately 9.5% higher than that of mediated by NLP (Fig. 8C), while the corresponding value for oleuropein reached almost 11.7% (Fig. 8D). The drug internalization facilitated by lipid membrane may occur through various routes, which are schematically shown in Fig. 8E (*56*).

Ex-NLP–Ba and Ex-NLP–Ole protect the integrity of BBB against αSN aggregates and cross the BBB in an in vitro model system

Aggregated αSN species can cause significant and detrimental changes to the integrity of the BBB and thus exacerbate PD (*57*). We therefore decided to investigate the effect of Ex-NLP–Ba and Ex-NLP–Ole on the model of BBB. We used human cerebral microvascular endothelial cell D3 (hCMEC/D3) cells to construct a cell model of the BBB. The cells were cultured on a Transwell plate until reaching a coherent monolayer culture. Figure S9A shows light microscope images of the cells on the Transwell for 4 days. To ensure the complete formation of the monolayer culture and the establishment of the tight junction between cells, the amount of transendothelial electrical resistance (TEER) was measured. The TEER gradually increased, indicating the formation of the monolayer culture. The fact that the TEER remained constant around days 6 to 7 further confirms the complete formation of the monolayer culture (fig. S9B). After the successful formation of the monolayer culture of hCMEC/D3, the cells were subjected to treatment with 15% αSN 24-hour–aggregated αSN formed in the presence or absence of Ex or Ex-NLP–Ba and Ex-NLP–Ole hybrids. TEER values were measured for a period of 72 hours. As shown in Fig. 9 and fig. S10, the TEER values initially decreased at a faster rate when αSN aggregated species were present alone compared to when Ex (fig. S10, A and B), Ex-NLP–Ba (Fig. 9, A and B), or Ex-NLP–Ole (Fig. 9, C and D) was present. However, the downward trend in TEER values was less steep when Ex were present, and after 72 hours, the TEER value was closer to the control value compared to the αSN alone group.

Delivery of drugs to the brain is a major obstacle due to the BBB (*58, 59*). Hence, we aimed to examine whether the hybrids could transport baicalein or oleuropein through our BBB model. After establishing a monolayer culture (fig. S9), we used Ex-NLP hybrids to examine the transfer of drugs across the BBB model. The findings demonstrated that after 8 hours, Ex-NLP hybrids were able to transport approximately 16 and 18% of baicalein and oleuropein, respectively, across the BBB model (Fig. 9E). Note that the very low solubility of free baicalein and oleuropein prevents us from measuring transport in these states, highlighting further the importance of using drug transport vehicles such as Ex-NLP hybrids. There may be different pathways for drug passage through the BBB, mediated by Ex-NLP, which are schematically illustrated in Fig. 9F.

Ex-NLP hybrids containing drugs moderated the wound-healing function of brain microvascular endothelial cells against αSN

The cellular migration of hCMEC/D3 cells was evaluated (*57*) through the implementation of a wound-healing assay (Fig. 10). The untreated cells exhibited a coherent and collective migration, maintaining intercellular connections. Conversely, when subjected to aggregated species of αSN treatment, the cells displayed individualized migration, which is deemed unsuitable for the processes of wound healing and endothelial cell migration. On the other hand, cells subjected to various treatment conditions, including Ex, Ex-NLP–Ba, and Ex-NLP–Ole, demonstrated a sheet migration pattern similar to that of the control. The treatment groups exhibited a notable capacity to partially restore cell cohesion and collective movement, thereby manifesting behavior akin to that of the control group. While the extent to which the scratch space was filled varied across the three treatment groups, all treatments effectively hindered cell detachment and individual cell migration toward the scratch space to some extent (Fig. 10A). The results were quantified as residual wound area (Fig. 10B) and the extent of wound closure after 24 and 48 hours (Fig. 10, C and D).

DISCUSSION

The use of carriers to effectively deliver drugs to the brain is a major global challenge due to the brain's complexity and crucial role in maintaining life. As part of our ongoing studies on the use of zwitterionic NLPs as effective carriers for treating PD due to their impacts on αSN fibrillation and neurotoxicity (*7*, *14*, *17*), here, we developed a nanosystem using Ex to enhance the efficiency of NLP. This nanosystem enjoys the general advantages of NLP systems such as biocompatibility, the ability to incorporate/encapsulate a variety of molecules, and low immunogenicity. In addition, Ex are naturally occurring carriers and can directly interact with cell surface receptors, and fuse to the cell membrane; therefore, their hybridization with liposomes aids in the competent internalization of the cargo into the cells. However, there is a concern that the hybridization process using the freeze-thawing method may disturb the characteristics of these two carriers and their cargo. Here, using FTIR, SDS-PAGE, FRET, intrinsic fluorescence, the scavenging activity of ROS, and other approaches, we demonstrate that freeze-thawing does not compromise this process.

Both Ex-NLP–Ba and Ex-NLP–Ole were found to decrease the extent of αSN fibrillation. The key to this is probably the interaction of αSN with either the lipid bilayer of NLP/Ex, the exosomal protein, and/or the small molecules, i.e., baicalein and oleuropein. We propose that a combination of all these interactions is involved in reducing the extent of fibrillation. However, the interaction of αSN monomer, oligomer, or fibrils with baicalein and oleuropein may differ due to specific binding modes, the strength of interactions, and the regions of the protein/aggregates they target. The variations in such interactions underscore the nuanced nature of their disruption mechanisms. During the fibrillation process, when treating

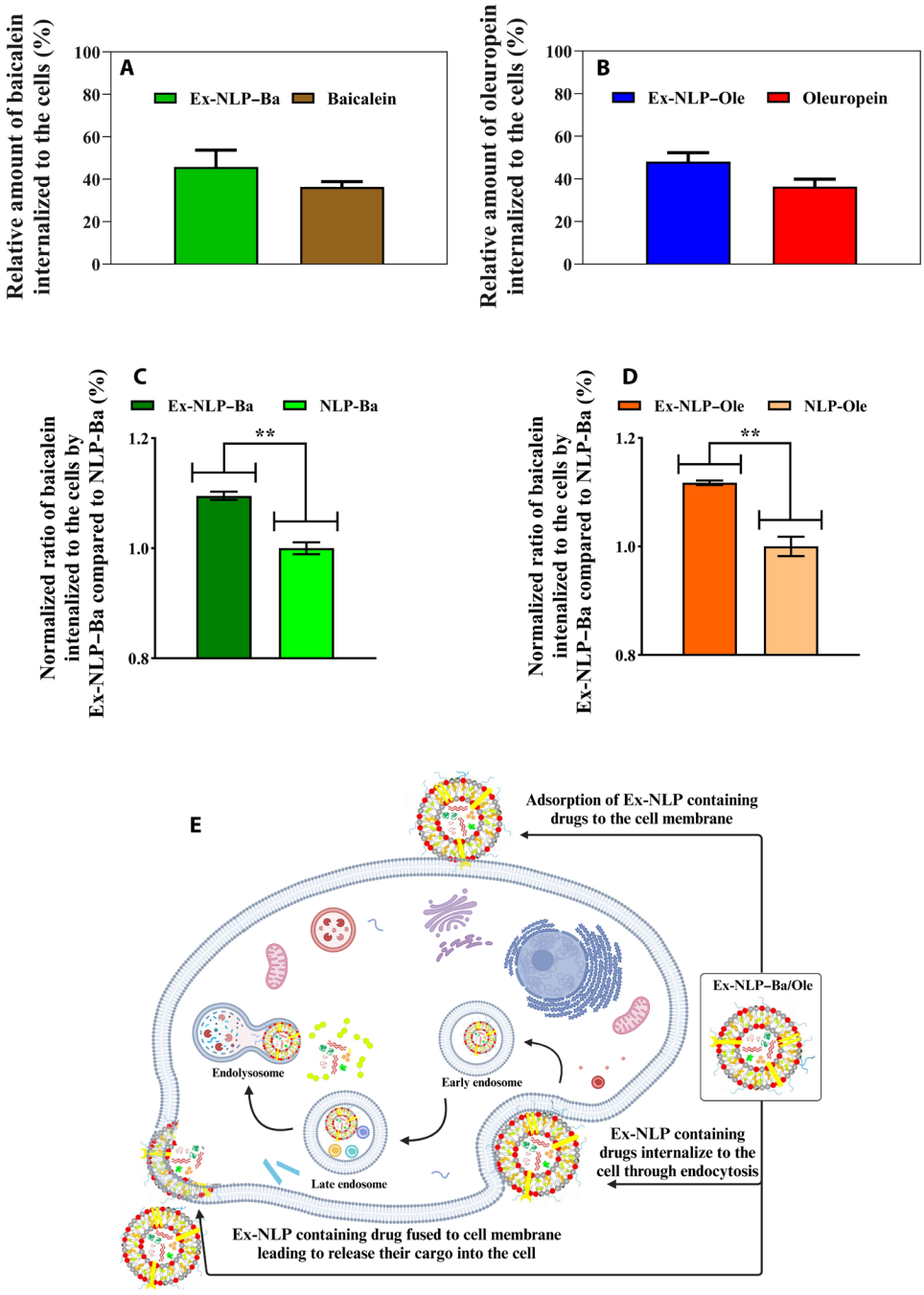

Fig. 8. Drug internalization mediated by Ex-NLP hybrids and NLPs into SHSY5Y cells. Internalization of baicalein (**A**) and oleuropein (**B**) through Ex-NLP hybrids into the SHSY5Y cells. The amount of baicalein or oleuropein (in the Ex-NLP hybrids or their free form) that entered the cells was normalized by their amount in the supernatants, and their internalized amount relative to their amount in the supernatant is represented. Baicalein and oleuropein may enter the cells through Ex-NLP hybrids. The small molecules (**C**) baicalein and (**D**) oleuropein are internalized more by Ex-NLP hybrids than by NLP. The concentration of drugs in each carrier was 100 μM and the ratio of Ex:NLP was 1:20. The percentage of the drugs entered into the cells was normalized to the total amount of drugs treated on the cells, and then the amount of drugs introduced by Ex-NLP hybrids was normalized to their amount by those of NLPs ($N = 3$, means ± SD, $^{**}P < 0.01$). (**E**) Schematic illustration of drug transport into the cells via the cell membrane (created with BioRender.com). Ex-NLP may adsorb to the surface of the cells, and the components of the cell membrane destabilize their membrane, allowing drugs to be released and taken up by the cell, or Ex-NLP may be internalized through endocytosis, where their membrane can form endosomes that are ultimately delivered to the lysosome or can become unstable and release the drug into the cytoplasm, or drugs can be released into the cytoplasm by fusing Ex-NLP with the cell membrane.

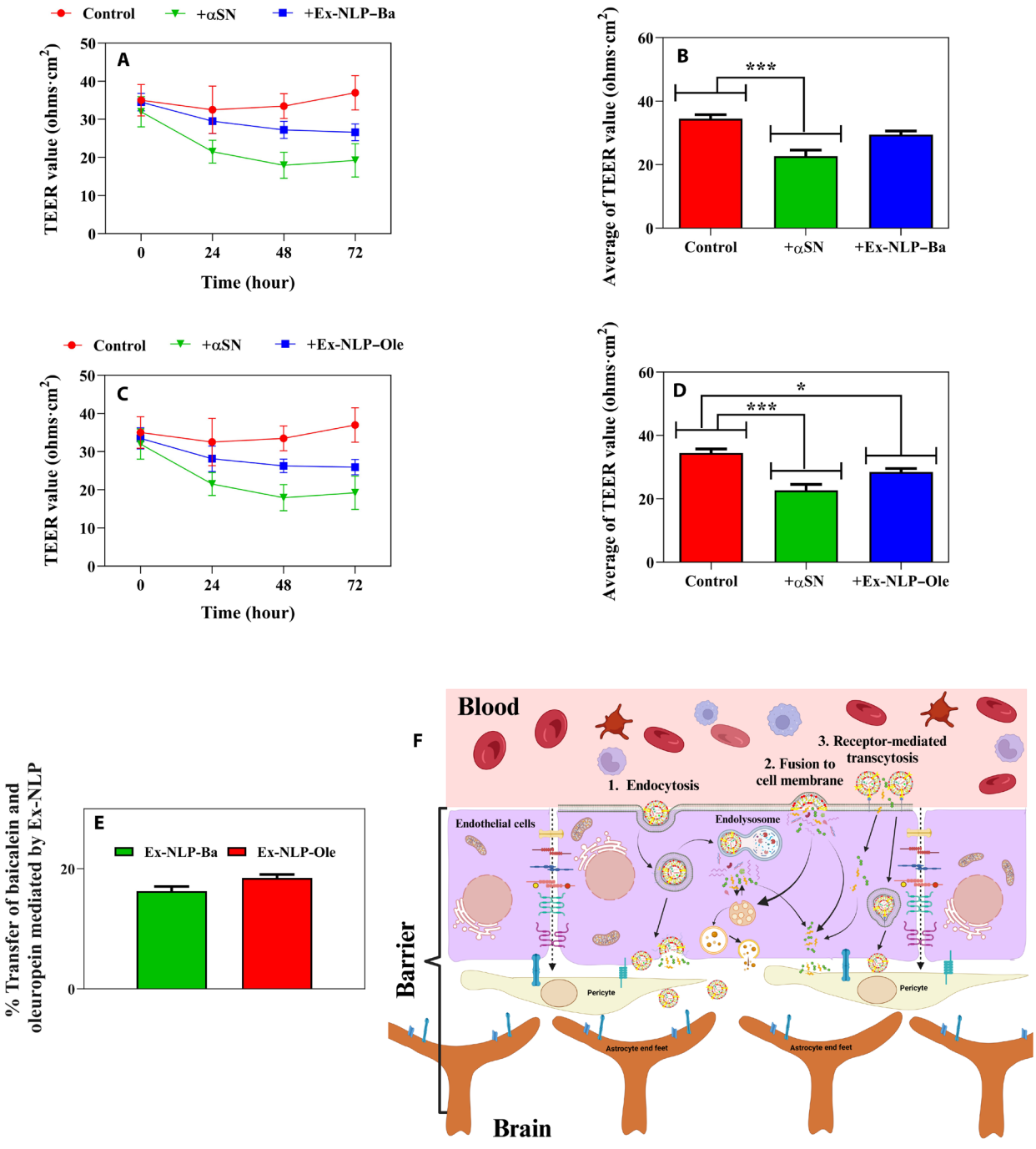

Fig. 9. TEER measurement of the BBB model in the presence of preformed 24hour–aggregated species of αSN (70 μM) without/with Ex-NLP–Ba and Ex-NLP–Ole hybrids (100 μM based on the small molecules concentration in the hybrids 1:20 Ex:NLP ratio), as well as the BBB crossing assessment. (**A** and **C**) TEER values over 72 hours for hCMEC/D3 cells treated with Ex-NLP–Ba (A) and Ex-NLP–Ole (C). (**B** and **D**) The average TEER values between different hours (0, 24, 48, and 72 hours) for Ex-NLP–Ba (B) and Ex-NLP–Ole (D) (*$P < 0.05$ and ***$P < 0.001$). (**E**) Ex-NLP hybrid–mediated crossing of baicalein or oleuropein through the BBB. A complete monolayer culture of hCMEC/D3 cells was established on a Transwell, and then Ex-NLP–Ba and Ex-NLP–Ole were added to the apical part, and the passage of baicalein and oleuropein was measured in the lower part. (**F**) Schematic illustration of Ex-NLP–mediated drug passage through the BBB (made in BioRender.com): (1) Ex-NLP–containing drugs may pass through the BBB via endocytosis-exocytosis or enter the endolysosomal system through the early and late endosome process. The drugs may eventually be degraded or transported inside the cell, crossing the cell directly. Alternatively, they might enter the exosome biogenesis process and become packed into multiple vesicular bodies, leading to the formation of the intraluminal body, ultimately exiting the cell via Ex. (2) Ex-NLP may fuse with BBB endothelial cells, releasing drugs into the cells. Consequently, the drugs may either be degraded inside the cells, directly cross the cells, or enter the Ex biogenesis cycle and cross the cells through Ex. (3) Ex-NLP may enter the cells through the receptor-mediated endocytosis system and pass through the BBB. It is also possible for drugs to reach the BBB with the support of Ex-NLP, where some drugs may be released, and directly enter the cells and pass through the BBB.

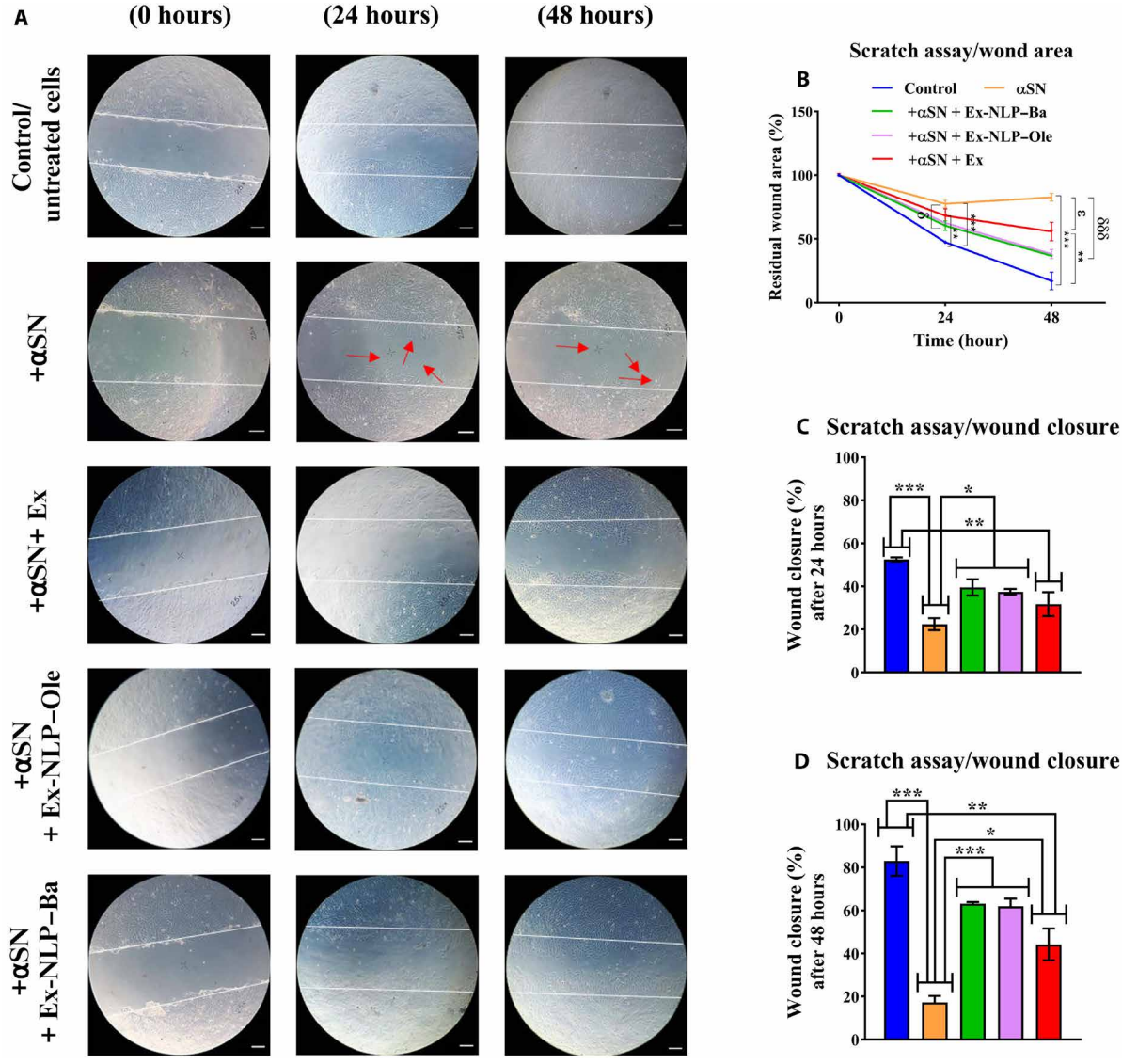

Fig. 10. In vitro scratch assay for wound healing. hCMEC/D3 cells were expanded to their maximum confluent density, scraped, and then subjected to various treatments. (**A**) The morphology of hCMEC/D3 cells for untreated cells (control), treated cells with preformed aggregates species of αSN in the absence or the presence of Ex, Ex-NLP–Ba, and Ex-NLP–Ole. Arrows indicate individual cells exhibiting random motions. (**B**) Quantitative evaluation of the remaining scratched area (* indicates significant differences between untreated and treated groups, δ indicates significant differences between preformed αSN aggregates species in the absence or the presence of Ex-NLP–Ba and Ex-NLP–Ole, and ε indicates significant differences between preformed αSN aggregates species in the absence or the presence of Ex). (**C**) Percentage of wound healing after 24 and (**D**) 48 hours. Using ImageJ software and Eqs. 4 and 5, the scratched area and wound closure were quantified. * indicates significant differences between selected treatments (means ± SD, $^{\delta,\varepsilon,}$ *$P \leq 0.05$, **$P \leq 0.01$, and *** and $^{\delta\delta\delta}P \leq 0.001$). Scale bars, 100 μm.

with Ex-NLP–Ba or Ex-NLP–Ole, we did not observe a notable delay in the nucleation phase, which indicates that during the early stages of fibrillation, baicalein and oleuropein are not accessible for interaction with αSN. The extent of interaction with αSN is a crucial determinant of the effectiveness of our nanosystems in mitigating neurodegenerative processes. Although direct quantification of this interaction remains challenging, our experimental design and results provide valuable insights. Our hybrids have demonstrated a significant impact on inhibiting αSN aggregation and promoting disaggregation, highlighting the importance of the specificity and strength of interactions. These findings support the potential of our nanosystem as a promising tool for combating αSN-associated neurodegeneration. Future studies could explore advanced techniques for a more detailed understanding of the nanosystems' interaction dynamics with αSN, further enhancing the comprehensive evaluation of their therapeutic potential. Using nuclear magnetic resonance spectroscopy, TEM, and circular dichroism thermal scanning, we have previously shown that αSN interacts with neutral NLPs through its N terminus, which takes place during the fibrillization process (*17*). Moreover, we and others have previously shown that baicalein may have covalent and/or noncovalent interaction with αSN (*7*, *47*, *48*). Oleuropein is also shown to interact with αSN in its

monomeric or aggregated forms (*16*, *49*, *50*). These interactions lead to the inhibition of fibrillation as well as the depolymerization of mature fibrils (*7*, *16*). Nevertheless, these small molecules face challenges related to hydrophobicity, low solubility, stability, and bioavailability, making them unsuitable for use in aquatic systems. Liposome-based nanosystems, however, effectively address these limitations, enhancing their efficiency and preserving their therapeutic potential for NDs (*7*). It is established that αSN interacts with phospholipid membranes through its N-terminal region. Furthermore, as αSN tends to interact with many proteins (*60*), here, we decided to investigate whether there is any interaction between exosomal protein and αSN as well. Moreover, the protein-protein interaction may cause the path of fibrillation to deviate. Therefore, using an in silico study, we found that αSN might also interact with Ex by binding to exosomal proteins or its membrane. The effects of Ex-NLP–Ba and Ex-NLP–Ole on the secondary nucleation further confirm the interaction of αSN with these materials. In addition, while NLP or Ex alone cannot depolymerize mature fibrils (*17*), we have shown that both Ex-NLP–Ba and Ex-NLP–Ole do, confirming previous observations that both baicalein and oleuropein can interact with aggregated species of αSN leading to disaggregate them (*7*, *16*). The mechanisms of disaggregation of αSN by baicalein have been discussed elsewhere, where the breakdown of fibrils due to their interaction by baicalein does not only happen at the fibril ends, as anticipated, but also occurs within internal regions, i.e., both exo- and endo-based disaggregation. This suggests the intercalation of baicalein, which has numerous hydrogen bond donors and acceptors, into the β sheet structure of the fibril, leading to the production of monomers and (likely off-pathway) oligomers (*47*). The critical structures in baicalein, including vicinal dihydroxyphenyl groups, and hydroxyl groups play essential roles in depolymerization (*61*). Moreover, the mechanisms of disruptive effects of baicalein on αSN fibrils depend on their polymorphism, through which baicalein disrupts the wild-type αSN fibril by targeting the E46-K80 salt-bridge and β sheets. It binds to the N-terminal, middle, and C-terminal residues of the wild-type αSN fibrils through aromatic interactions, hydrophobic interactions, and H-bonding interactions. In addition, it induces remodeling of the inter-protofilament interface (*62*). Oleuropein has also been shown not to solubilize the aggregates but to transform them into smaller assemblies resembling the off-pathway oligomers (*49*).

Our study also revealed that Ex-NLP–Ba and Ex-NLP–Ole both have the ability to scavenge free radicals from the environment and exhibit antioxidant activity. While zwitterionic NLPs lack antioxidant activity (*17*), baicalein (*14*, *16*) and oleuropein have antioxidant properties. These data suggest that the antioxidant activity of Ex-NLP–Ba and Ex-NLP–Ole may be attributed to the presence of small molecules within their structure. Despite their efficacy as drug carriers due to biocompatibility, zwitterionic NLPs inherently lack antioxidant activity due to the net neutral nature of zwitterionic lipids, which hinders their ability to effectively scavenge free radicals (antioxidant action involves donating electrons or hydrogen atoms, a capacity lacking in such lipids). In contrast, baicalein and oleuropein, with specific phenolic structural features, contribute to the antioxidant properties of the developed hybrids by providing the needed capacity for neutralizing free radicals. The antioxidant mechanism of phenolic compounds like baicalein and oleuropein involves processes such as hydrogen atom transfer, sequential proton loss electron transfer, electron transfer–proton transfer, transfer of a single electron, and chelation of transition metals. As regards baicalein, the sequential proton loss electron transfer mechanism has been shown to play a more considerable role in aqueous solution (*63*). The chemical structure of baicalein includes multiple phenolic hydroxyl groups, which confer potent free radical scavenging capabilities (*64*). These hydroxyl groups can effectively neutralize ROS and prevent oxidative damage to biomolecules. Baicalein can also directly interact with ROS, acting as a direct antioxidant (*65*). In addition, baicalein has been shown to enhance the activity of endogenous antioxidant enzymes, further contributing to its overall antioxidant effects (*64*). The incorporation of baicalein into our nanosystem provides an additional layer of protection against oxidative stress. Similar to baicalein, oleuropein has notable antioxidant properties. Its chemical structure includes a hydroxy-tyrosol moiety, responsible for its free radical scavenging activity. Oleuropein has been reported to protect cells from oxidative stress by modulating various signaling pathways and reducing ROS levels. In addition, it can chelate metal ions, further preventing the generation of harmful free radicals (*66*).

We also found that these hybrids are better at internalizing drugs into cells than Ex-free NLPs. Several mechanisms have been proposed for drug internalization into cells through liposome membranes. Because both baicalein and oleuropein are hydrophobic, endocytosis is likely the most effective mechanism for their entry into the cell. Moreover, liposomes can absorb into the cell surface and be permeable, leading to the release of its content. On the other hand, during membrane fusion, baicalein and oleuropein molecules may remain trapped in the lipid bilayer and would only be released slowly over time (*56*, *67*). MSC-derived Ex also enhanced drug uptake through endocytosis, receptor interactions, and lipid bilayer fusion, allowing efficient cargo delivery into neuronal cells. Exosomal proteins may influence uptake, but cargo compatibility, cargo loading capacity, and intracellular trafficking complexities need careful consideration. MSC-derived Ex may have inherent targeting capabilities, homing to specific tissues or cell types, thereby optimizing drug delivery specificity. The nanosized Ex efficiently enter cells, facilitating targeted drug delivery and enhancing therapeutic impact in NDs.

We observed that the hybrid of Ex-NLP is capable of penetrating the BBB, and such penetration was relatively higher than that of Ex-free NLPs. The BBB acts as a natural defense mechanism against pathogens and other external factors, making it difficult for drugs to enter the brain (*68*). Hence, nanocarriers that can effectively bypass this barrier and transport drugs to the brain are crucial for developing effective therapies. Despite the fact that a small number of low molecular weight drugs are capable of penetrating the BBB, this remains a challenge. In this study, we found the capability of our developed hybrids to transport drugs through the BBB model. This offers proof of their effectiveness as a promising option for addressing ND. The mechanisms underlying this penetration involve several factors. First, NLPs, as lipid-based carriers, are known to interact effectively with cell membranes. The amphiphilic nature of the lipid bilayer allows them to merge with cell surfaces and through processes like endocytosis, facilitating drug internalization (*14*). Moreover, the incorporation of Ex, which are naturally occurring carriers, further enhances the efficiency of the nanosystem. Ex can directly interact with cell surface receptors and fuse with cell membranes, aiding in the internalization of the cargo into cells (*69*–*71*). The freeze-thawing method used for the hybridization process, as

characterized by FTIR, SDS-PAGE, FRET, intrinsic fluorescence, and scavenging activity of ROS, did not adversely affect the characteristics of the carriers or their cargo. To delve into the potential implications for the treatment of NDs, we note that effective drug delivery to the brain is important in developing therapies for such conditions. The ability of these hybrids to bypass the BBB model suggests their potential as a promising option for addressing NDs. Moreover, the presence of hybrids during αSN fibrillation reduced the destructive effects of αSN aggregates on wound healing, indicating a positive impact on cellular function. In the BBB, the cells are expected to move together to close the scratch space and to show a collective movement due to the existence of extracellular matrix (ECM) and strong connections (*57*). αSN prevents the normal closure of the scratched area and inhibits migration, perhaps because the cells move individually, but not in a sheet form. Here, in the presence of αSN aggregates, we observed an abnormal migration of endothelial cells. An individual cell moved and separated from the rest of the cells, which is probably due to the opening of the junction and the reduction or disintegration of the ECM around the cells, which can probably be due to the activation of the matrix metalloproteinases faced with αSN aggregates (*57*). For the cells treated with αSN aggregates preformed in the presence of Ex, Ex-NLP–Ba, and Ex-NLP–Ole, however, an improvement in the function and closing of the scratch area was detected, suggesting that these materials reduced the aggregate species of αSN, leading to the reduction of the movement of single cells into the scratch space and cause the BBB cells to stay connected together and so have a grouping migration. The presence of hybrids reduced the abnormal migration of endothelial cells.

In the end, our aim here was to enhance the natural qualities of the hybrids and improve drug effectiveness. This led to the successful fusion of the two different nanoparticles while maintaining their characters, e.g., both exosomal proteins and small molecules were retained within the hybrid. Figure S11 summarizes our results and interpretation. Improvement of such kinds of nanosystems provides more features in the treatment of PD. These nanosystems were checked here for the αSN fibrillation/neurotoxicity, and crossing through the BBB model, but the main purpose of creating this platform is for the broader purpose of PD, e.g., damaged neuron regeneration. The presence of MSC-derived Ex in this fusion led to an increase in the drug uptake by the neuronal cells. This system has a potential therapeutic approach for treating PD because of its broad applications including impeding the aggregation, enhancing drug internalization, and entering the beneficial compounds from the natural source to the cells.

MATERIALS AND METHODS

Materials

DPPC, PEG2000 PE, and a Mini-Extruder were from Avanti Polar Lipids Inc. (USA). Baicalein, oleuropein, ThT, MTT, 2′,7′-dichloro dihydrofluorescein diacetate (DCFH-DA), poly-L-lysine, gelatin, Griess reagent, and cholesterol were from Sigma-Aldrich (St Louis, MO). Fetal bovine serum (FBS) was from Biosera (Tehran, Iran). Antibiotics and RPMI 1640 medium, DMEM high glucose, and DMEM/F-12 (DMEM/Nutrient Mixture F-12) were from GibcoBRL (Life Technologies, Paisley, Scotland). Twenty-four–well Transwell inserts (0.4-μm pore size, polyester membrane) were from Plastics & Membrane Technology (SABEU, Germany).

hUC MSC isolation and characterization

Fresh umbilical cord tissue connected to the placenta junction (obtained from a healthy mother by cesarean delivery) was transferred to the laboratory under sterile conditions at 4°C, housed in a container containing phosphate-buffered saline (PBS) supplemented with antibiotics [ciprofloxacin (10 μg/ml), gentamicin (50 μg/ml), and amphotericin B (10 μg/ml)]. MSC extraction was performed within 4 to 6 hours. While the hUC is typically considered medical waste destined for disposal, we obtained prior consent from both parents and the hospital, following established protocols and guidelines set forth by the National Institutes of Genetic Engineering and Biotechnology Ethics Committee (IR.NIGEB.EC.1399.4.9.C). The MSC isolation procedure followed our previously established protocol using explant culture (*72*). Briefly, the tissue was washed two to three times with antibiotic-containing PBS. A part of the umbilical cord and the placenta junction was divided into 1- to 2-cm pieces and subjected to further washing. Then, the blood vessels were removed, and the exposed Wharton jelly was divided into 1- to 2-mm pieces. The pieces were placed on the bottom of 10-cm cell culture plates precoated with 0.1% poly-L-lysine and 1% gelatin and fixed using sterilized metal mesh grids which were placed on the tissue fragment. The samples were incubated for 5 to 10 min under sterile conditions (under the laminar hood) until the tissues were slightly dried and attached to the bottom of the plate. DMEM-F12 culture media supplemented with 15% FBS and 2% antibiotics was then added to the plate, after which it was incubated at 37°C, 90% humidity, and 5% CO_2 for 2 weeks. Every 3 days, half of the media was replaced with fresh complete culture media until reaching 80 to 90% confluency. The MSCs were dissociated from the tissue and spread around. In the third passage, the extracted cells from the umbilical cord were examined for surface marker expression using flow cytometry (see the Supplementary Materials for additional details).

hUC MSC–derived exosome purification and characterization

MSCs at passages 4 to 6 were cultured into serum-free media containing a mixture of RPMI 1640 and DMEM high glucose [80:20 (v/v)] (more details provided in the Supplementary Materials). To extract Ex, conditioned media obtained from 48 hours of cell incubation were collected and centrifuged at 2000*g* for 10 min followed by 16,000*g* for 30 min to remove dead cells and debris/apoptotic bodies, respectively. The supernatant was then passed through a 0.22-μm filter membrane and then subjected to Ex extraction using an Exo-spin kit (Cell Guidance System, Cambridge, UK). Ex extraction was based on polymer precipitation followed by size exclusion chromatography. The protein concentration of Ex was then quantified using a BCA kit and aliquots of Ex (400 μg/ml; based on protein assay) were flash-frozen using liquid nitrogen and stored at −80°C. Ex was then characterized using Western blot analysis, DLS using a Zetasizer (Malvern, UK), and TEM, as detailed in the Supplementary Materials.

Fabrication of hybrids of hUC MSC–derived exosome and NLPs

NLPs contained DPPC supplemented with 15% (mol/mol) cholesterol decorated with 10% (mol/mol) PEG2000 PE. Baicalein or oleuropein was incorporated at mol/mol ratios of 1:3 baicalein:phospholipids and 1:4 oleuropein:phospholipids. These NLPs were then fused with

Ex at three ratios of 1:10, 1:20, and 1:100 Ex:NLP (w/w) (see the Supplementary Materials for more details).

αSN preparation, fibrillation, seeding, and disaggregation

Human αSN was expressed in *Escherichia coli* BL21 (DE3) pLysS and purified by ion exchange chromatography. Purified αSN was dissolved in PBS containing 20 μM ThT, 100 μM EDTA, 100 μM phenylmethylsulfonyl fluoride, and 0.005% sodium azide (NaN_3), and then passed over a 0.22-μm filter. Protein concentration was calculated using a theoretical extinction coefficient at 280 nm of 0.412 mg^{-1} ml^{-1} cm^{-1}. Subsequently, 70 μM αSN was incubated at 37°C within a 96-well plate accompanied by a 3-mm-diameter glass bead under orbital shaking at 300 rpm. The kinetic of αSN fibrillation was monitored using ThT fluorescence intensity. Normalized ThT data were fitted on the Finke-Watzky two-step model (*73*). For secondary nucleation, seeds were generated by subjecting 48-hour preformed fibrils to a 5-min sonication using an ultrasonic bath sonicator (Bandelin Sonorex Ultrasonic baths Digital 10P, Germany) operating at 50% amplitude (*11*, *74*). For the disaggregation assay, αSN fibrils were incubated with Ex-NLP–Ba or Ex-NLP–Ole, and the ThT fluorescence intensity was recorded for 48 hours. Further details of the mentioned methods in this section are provided in the Supplementary Materials.

In Silico analysis

Potential interactions between αSN and Ex-NLP–Ba or Ex-NLP–Ole were assessed in silico. To this end, we used human αSN (PDB ID:1XQ8) and the fibril form of αSN (PDB ID:2N0A), which involves a 10-chain assembly of αSN monomers. In addition, we selected a subset of five αSN chains from 2N0A and considered them 5-chain aggregates. Protein-protein binding analysis was performed for exosomal markers and three αSN structures using the HDOCK server, which generated 100 docking models. The optimal protein-protein docking configurations were selected based on the lowest docking score and highest confidence score for each protein. The chosen models were visualized using PyMol to analyze molecular interactions and structural details. In addition, we used molecular docking (*75*) to evaluate the interaction of αSN aggregates with baicalein or oleuropein. See the Supplementary Materials for details.

The impact of Ex-NLP–Ba or Ex-NLP–Ole on αSN neurotoxicity

To assess the neurotoxicity of αSN in the absence and the presence of Ex-NLP hybrids containing drugs, mitochondrial metabolic activity of SHSY5Y cells using MTT assay (6×10^4 cells/ml in 96-well plates), intracellular ROS using DCFH-DA assay (10×10^4 cells/ml in 96-well plates), and NO production using Griess assay (15×10^4 cells per well in 12-well plates) was measured. To do so, SHSY5Y cells were cultured at a desired density in DMEM-F12 supplemented with penicillin (100 U/ml), streptomycin (100 μg/ml), and 10% FBS and incubated at 37°C in a humidified CO_2 incubator (90% humidity and 5% CO_2) for 24 hours. Cell viability, intracellular ROS, and NO were assessed as described in the Supplementary Materials.

Hemolysis assay

One hundred microliters of either Ex-NLP–Ba or Ex-NLP–Ole (final concentration of 100 μM based on the baicalein or oleuropein) was applied onto a blood agar plate and incubated at 37°C for 24 hours. One hundred microliters of 0.5 McFarland of *Bacillus Cereus* was cultured under the same conditions. The absence of observable hemolysis was taken as an indicator of biocompatibility.

Antioxidant activity of hybrids

The antioxidant activity of Ex-NLP–Ba and Ex-NLP–Ole was investigated by DPPH• measurement. Unless otherwise stated, all hybrids were applied at a concentration corresponding to 100 μM of the incorporated baicalein or oleuropein at a 1:20 molar ratio of Ex:NLP. One hundred microliters of each of the hybrids, as well as Ex at two concentrations of 20 and 10 μg/ml, was mixed with 200 μl of DPPH• (100 μM) and incubated for 30 min at room temperature in the dark. The amount of antioxidant activity was monitored by absorption at 517 nm and the percentage of antioxidant activity was obtained as follows

$$\%\ \text{of antioxidant activity} = \frac{\text{OD (517 nm) of control} - \text{OD (517 nm) of sample}}{\text{OD (517 nm) of control}} \times 100 \quad (1)$$

The control was [DPPH•] and the samples were [DPPH•] in the presence of Ex-NLP–Ba, Ex-NLP–Ole, and Ex.

Drug internalization studies

To explore the potential of Ex-NLP–Ba and Ex-NLP–Ole as carriers for delivering drugs to cells, we performed cellular uptake experiments. For this purpose, 100 μM of each hybrid, as well as baicalein and oleuropein (100 μM), was added to SHSY5Y cells in a serum-free media and incubated for 4 hours. Then, the cells were washed twice using PBS, trypsinized and lysed with 2% Triton X-100, dissolved in methanol, incubated for 30 min at 37°C, and then centrifuged at 10,000 rpm for 10 min. The absorption of the supernatant was measured at 277 nm for baicalein and 230, 248, 269, and 272 nm for oleuropein (blanked with untreated cells with the same conditions). The average concentration of drugs present inside the cells was normalized to the concentration in the supernatant.

In vitro model of BBB

To establish an in vitro model of the BBB, hCMEC/D3 cells were cultured at a density of 5×10^4 cells per well in RPMI 1640 supplemented with 5% FBS, 1.4 μM hydrocortisone, and 2 mM GlutaMAX onto the apical section of a Transwell 24-well plate (precoated with 0.1% collagen type I) with a pore size of 0.4 μm and a diameter insert of 6.5 mm, providing a growth area of 0.33 cm^2 per well (Corning Incorporated Costar, USA). The plate was then incubated in a humidified CO_2 incubator (95% humidity and 5% CO_2) at 37°C. Subsequently, the Transepithelial/TEER value (in ohms per square centimeter) of the monolayer cells was monitored for consecutive days using the EVOM2 (World Precision Instruments, USA). Measurements were taken until the resistance level reached a consistent value over two consecutive days (approximately 35 ohms·cm^2), demonstrating the successful formation of a cellular monolayer. Each day, the culture media were renewed by replacing it with fresh media after washing the cells twice with PBS. Following the media change, the electrical resistance of the cells was measured.

The TEER value for each well was calculated using the following formula

$$\text{TEER value} = (\text{TEERcell} - \text{TEERblank}) \times \text{cell growth area} \quad (2)$$

where TEERcell represents the electrical resistance of the well including the cells, and TEERblank is the electrical resistance of the empty wells.

Assessing the impact of hybrids on αSN's destructive effect on the BBB model through TEER measurement

To evaluate the integrity of the BBB model in the monolayer culture model toward αSN aggregated species (24 hours), once the TEER value (in ohms per square centimeter) stabilized at a consistent level, the cells were treated with 15% of 24-hour–aggregated species of αSN preformed without or with Ex-NLP–Ba and Ex-NLP–Ole hybrids at a concentration of 100 μM. The TEER values were subsequently monitored every 24 hours for a duration of 72 hours. This involved exchanging the upper culture medium of the insert with fresh medium after every 24-hour measurement session.

In vitro assessment of BBB permeability for drugs containing hybrids

The hCMEC/D3 cells were cultured on the insert of a Transwell 24-well plate at a density of 5×10^4 cells per well, creating a complete monolayer culture, followed by the treatment with 100 μM of Ex-NLP–Ba and Ex-NLP–Ole in serum-free media. After an 8-hour incubation period, the levels of baicalein and oleuropein were measured by absorbance in both the upper and lower culture media. A sample containing only the culture medium without any additional substances was used as blank. The percentage of small molecules that successfully crossed the BBB model was calculated as follows

$$\%\ \text{of passed small molecules} = \frac{\text{Amount of small molecules in the lower reservior}}{\text{Amount of small molecules added to the upper reservior}} \times 100 \quad (3)$$

Scratch assay for evaluating the wound-healing potential of hCMEC/D3 cells

hCMEC/D3 cells at a density of 5×10^4 cells/ml were cultured onto 96-well plates and incubated at 37°C. Once the cells covered the surface of the plate, a straight horizontal line was created on the cell-coated surface by making a scratch using a sterile pipette tip, and the media were replaced with fresh serum-free media, after washing the cells two times with PBS. The cells were then treated with αSN aggregated in the absence or the presence of Ex or Ex-NLP–containing drug hybrids and incubated for up to 48 hours. The untreated cells were used as a control. The extent of cellular migration was assessed at both 24 and 48 hours after treatment. The area of the scratched region was measured using ImageJ software, and the percentages of the scratched area and closure of the scratched region were calculated as follows

$$\%\ \text{scratched field area} = \frac{A_{t\Delta h}}{A_{t0}} \times 100\,\% \quad (4)$$

$$\%\ \text{scratched field closure} = \left[\frac{A_{t0} - A_{t\Delta h}}{A_{t0}}\right] \times 100\,\% \quad (5)$$

Here, "A_{t0}" represents the scratch wound's initial area, while "$A_{t\Delta h}$" corresponds to the scratch wound's area after a time interval of either 24 or 48 hours.

Statistical analysis

All experiments were conducted in triplicate, and the results are presented as means ± SD. One-way analysis of variance (ANOVA) was used to determine the statistical significance within the groups. The unpaired Student's *t* test was also applied to establish significant differences between the groups, with a *P* value of ≤0.05 considered significant.

Supplementary Materials

This PDF file includes:

Supplementary Text
Figs. S1 to S11
Tables S1 and S2

REFERENCES AND NOTES

1. N. P. Visanji, A. E. Lang, G. G. Kovacs, Beyond the synucleinopathies: Alpha synuclein as a driving force in neurodegenerative comorbidities. *Transl. Neurodegener.* **8**, 28 (2019).
2. H. McCann, C. H. Stevens, H. Cartwright, G. M. Halliday, α-Synucleinopathy phenotypes. *Parkinsonism Relat. Disord.* **20**, S62–S67 (2014).
3. Y. X. Xie, N. N. Naseri, J. Fels, P. Kharel, Y. Na, D. Lane, J. Burré, M. Sharma, Lysosomal exocytosis releases pathogenic α-synuclein species from neurons in synucleinopathy models. *Nat. Commun.* **13**, 4918 (2022).
4. K. C. Luk, V. Kehm, J. Carroll, B. Zhang, P. O'Brien, J. Q. Trojanowski, V. M.-Y. Lee, Pathological α-synuclein transmission initiates Parkinson-like neurodegeneration in nontransgenic mice. *Science* **338**, 949–953 (2012).
5. M. Teil, M.-L. Arotcarena, E. Faggiani, F. Laferriere, E. Bezard, B. Dehay, Targeting α-synuclein for PD Therapeutics: A pursuit on all fronts. *Biomolecules* **10**, 391 (2020).
6. M. Kurnik, C. Sahin, C. B. Andersen, N. Lorenzen, L. Giehm, H. Mohammad-Beigi, C. M. Jessen, J. S. Pedersen, G. Christiansen, S. V. Petersen, R. Staal, G. Krishnamurthy, K. Pitts, P. H. Reinhart, F. A. A. Mulder, S. Mente, W. D. Hirst, D. E. Otzen, Potent α-synuclein aggregation inhibitors, identified by high-throughput screening, mainly target the monomeric state. *Cell Chem. Biol.* **25**, 1389–1402.e9 (2018).
7. F. Aliakbari, H. Mohammad-Beigi, S. Abbasi, N. Rezaei-Ghaleh, F. Lermyte, S. Parsafar, S. Becker, A. P. Tafreshi, P. B. O'Connor, J. F. Collingwood, G. Christiansen, D. S. Sutherland, P. H. Jensen, D. Morshedi, D. E. Otzen, Multiple protective roles of nanoliposome-incorporated baicalein against α-synuclein aggregates. *Adv. Funct. Mater.* **31**, 2007765 (2021).
8. S. Parsafar, F. Aliakbari, S. S. Seyedfatemi, Z. Najarzadeh, H. Hourfar, H. Bardania, M. Farhadpour, M. Mohammadi, D. Morshedi, Insights into the inhibitory mechanism of skullcapflavone II against α-synuclein aggregation and its mediated cytotoxicity. *Int. J. Biol. Macromol.* **209**, 426–440 (2022).
9. S. Parsafar, Z. Nayeri, F. Aliakbari, F. Shahi, M. Mohammadi, D. Morshedi, Multiple neuroprotective features of *Scutellaria pinnatifida*-derived small molecule. *Heliyon* **6**, e04737 (2020).
10. D. Morshedi, T. S. Kesejini, F. Aliakbari, R. Karami-Osboo, M. Shakibaei, A. T. Marvian, M. Khalifeh, M. Soroosh, Identification and characterization of a compound from *Cuminum cyminum* essential oil with antifibrilation and cytotoxic effect. *Res. Pharm. Sci.* **9**, 431–443 (2014).
11. D. Morshedi, F. Aliakbari, A. Tayaranian-Marvian, A. Fassihi, F. Pan-Montojo, H. Pérez-Sánchez, Cuminaldehyde as the major component of *Cuminum cyminum*, a natural aldehyde with inhibitory effect on α-synuclein fibrillation and cytotoxicity. *J. Food Sci.* **80**, H2336–H2345 (2015).
12. N. Lorenzen, S. B. Nielsen, Y. Yoshimura, B. S. Vad, C. B. Andersen, C. Betzer, J. D. Kaspersen, G. Christiansen, J. S. Pedersen, P. H. Jensen, F. A. A. Mulder, D. E. Otzen, How epigallocatechin gallate can inhibit α-synuclein oligomer toxicity in vitro. *J. Biol. Chem.* **289**, 21299–21310 (2014).
13. M. Sashourpour, S. Zahri, T. Radjabian, V. Ruf, F. Pan-Montojo, D. Morshedi, A study on the modulation of α-synuclein fibrillation by *Scutellaria pinnatifida* extracts and its neuroprotective properties. *PLOS ONE* **12**, e0184483 (2017).
14. F. Aliakbari, A. A. Shabani, H. Bardania, H. Mohammad-Beigi, A. Tayaranian Marvian, F. Dehghani Esmatabad, A. A. Vafaei, S. A. Shojaosadati, A. A. Saboury, G. Christiansen, D. E. Otzen, D. Morshedi, Formulation and anti-neurotoxic activity of baicalein-incorporating neutral nanoliposome. *Colloids Surf. B Biointerfaces* **161**, 578–587 (2018).
15. M. Malakouti-Nejad, H. Bardania, F. Aliakbari, A. Baradaran-Rafii, E. Elahi, D. Monti, D. Morshedi, Formulation of nanoliposome-encapsulated bevacizumab (Avastin): Statistical optimization for enhanced drug encapsulation and properties evaluation. *Int. J. Pharm.* **590**, 119895 (2020).

16. H. Mohammad-Beigi, F. Aliakbari, C. Sahin, C. Lomax, A. Tawfike, N. P. Schafer, A. Amiri-Nowdijeh, H. Eskandari, I. M. Møller, M. Hosseini-Mazinani, G. Christiansen, J. L. Ward, D. Morshedi, D. E. Otzen, Oleuropein derivatives from olive fruit extracts reduce α-synuclein fibrillation and oligomer toxicity. *J. Biol. Chem.* **294**, 4215–4232 (2019).
17. F. Aliakbari, H. Mohammad-Beigi, N. Rezaei-Ghaleh, S. Becker, F. Dehghani Esmatabad, H. A. Eslampanah Seyedi, H. Bardania, A. Tayaranian Marvian, J. F. Collingwood, G. Christiansen, M. Zweckstetter, D. E. Otzen, D. Morshedi, The potential of zwitterionic nanoliposomes against neurotoxic α-synuclein aggregates in Parkinson's Disease. *Nanoscale* **10**, 9174–9185 (2018).
18. M. F. Pittenger, A. M. Mackay, S. C. Beck, R. K. Jaiswal, R. Douglas, J. D. Mosca, M. A. Moorman, D. W. Simonetti, S. Craig, D. R. Marshak, Multilineage potential of adult human mesenchymal stem cells. *Science* **284**, 143–147 (1999).
19. C. Théry, K. Ewa, Minimal information for studies of extracellular vesicles 2018 (MISEV2018): A position statement of the International Society for Extracellular Vesicles and update of the MISEV2014 guidelines. *J. Extracell Vesicles* **7**, 1535750 (2018).
20. F. J. Vizoso, N. Eiro, S. Cid, J. Schneider, R. Perez-Fernandez, Mesenchymal stem cell secretome: Toward cell-free therapeutic strategies in regenerative medicine. *Int. J. Mol. Sci.* **18**, 1852 (2017).
21. M. Thompson, S. H. J. Mei, D. Wolfe, J. Champagne, D. Fergusson, D. J. Stewart, K. J. Sullivan, E. Doxtator, M. Lalu, S. W. English, J. Granton, B. Hutton, J. Marshall, A. Maybee, K. R. Walley, C. Dos Santos, B. Winston, L. McIntyre, Cell therapy with intravascular administration of mesenchymal stromal cells continues to appear safe: An updated systematic review and meta-analysis. *EClinicalMedicine* **19**, 100249 (2020).
22. C. Théry, Exosomes: Secreted vesicles and intercellular communications. *F1000 Biol. Rep.* **3**, 15 (2011).
23. S. M. Davidson, J. A. Riquelme, K. Takov, J. M. Vicencio, C. Boi-Doku, V. Khoo, C. Doreth, D. Radenkovic, S. Lavandero, D. M. Yellon, Cardioprotection mediated by exosomes is impaired in the setting of type II diabetes but can be rescued by the use of non-diabetic exosomes in vitro. *J. Cell. Mol. Med.* **22**, 141–151 (2018).
24. M. Kou, L. Huang, J. Yang, Z. Chiang, S. Chen, J. Liu, L. Guo, X. Zhang, X. Zhou, X. Xu, X. Yan, Y. Wang, J. Zhang, A. Xu, H.-F. Tse, Q. Lian, Mesenchymal stem cell-derived extracellular vesicles for immunomodulation and regeneration: A next generation therapeutic tool? *Cell Death Dis.* **13**, 580 (2022).
25. R. J. Simpson, J. W. E. Lim, R. L. Moritz, S. Mathivanan, Exosomes: Proteomic insights and diagnostic potential. *Expert Rev. Proteomics* **6**, 267–283 (2009).
26. H. Valadi, K. Ekström, A. Bossios, M. Sjöstrand, J. J. Lee, J. O. Lötvall, Exosome-mediated transfer of mRNAs and microRNAs is a novel mechanism of genetic exchange between cells. *Nat. Cell Biol.* **9**, 654–659 (2007).
27. C. Frühbeis, D. Fröhlich, W. P. Kuo, J. Amphornrat, S. Thilemann, A. S. Saab, F. Kirchhoff, W. Möbius, S. Goebbels, K. A. Nave, A. Schneider, M. Simons, M. Klugmann, J. Trotter, E.-M. Krämer-Albers, Neurotransmitter-triggered transfer of exosomes mediates oligodendrocyte–Neuron communication. *PLOS Biol.* **11**, e1001604 (2013).
28. C. Frühbeis, D. Fröhlich, W. P. Kuo, E.-M. Krämer-Albers, Extracellular vesicles as mediators of neuron-glia communication. *Front. Cell. Neurosci.* **7**, 182 (2013).
29. M. Record, K. Carayon, M. Poirot, S. Silvente-Poirot, Exosomes as new vesicular lipid transporters involved in cell–cell communication and various pathophysiologies. *Biochim. Biophys. Acta* **1841**, 108–120 (2014).
30. Q. Liu, S. Li, A. Dupuy, H. Le Mai, N. Sailliet, C. Logé, J. M. H. Robert, S. Brouard, Exosomes as new biomarkers and drug delivery tools for the prevention and treatment of various diseases: Current perspectives. *Int. J. Mol. Sci.* **22**, 7763 (2021).
31. D. G. Phinney, M. F. Pittenger, Concise review: MSC-derived exosomes for cell-free therapy. *Stem Cells* **35**, 851–858 (2017).
32. X. Wang, Y. Chen, Z. Zhao, Q. Meng, Y. Yu, J. Sun, Z. Yang, Y. Chen, J. Li, T. Ma, H. Liu, Z. Li, J. Yang, Z. Shen, Engineered exosomes with ischemic myocardium-targeting peptide for targeted therapy in myocardial infarction. *J. Am. Heart Assoc.* **7**, e008737 (2018).
33. B.-C. Yang, M.-J. Kuang, J.-Y. Kang, J. Zhao, J.-X. Ma, X.-L. Ma, Human umbilical cord mesenchymal stem cell-derived exosomes act via the miR-1263/Mob1/Hippo signaling pathway to prevent apoptosis in disuse osteoporosis. *Biochem. Biophys. Res. Commun.* **524**, 883–889 (2020).
34. W. Liu, L. Li, Y. Rong, D. Qian, J. Chen, Z. Zhou, Y. Luo, D. Jiang, L. Cheng, S. Zhao, F. Kong, J. Wang, Z. Zhou, T. Xu, F. Gong, Y. Huang, C. Gu, X. Zhao, J. Bai, F. Wang, W. Zhao, L. Zhang, X. Li, G. Yin, J. Fan, W. Cai, Hypoxic mesenchymal stem cell-derived exosomes promote bone fracture healing by the transfer of miR-126. *Acta Biomater.* **103**, 196–212 (2020).
35. K. H. Haider, B. Aramini, Mircrining the injured heart with stem cell-derived exosomes: An emerging strategy of cell-free therapy. *Stem Cell Res. Ther.* **11**, 23 (2020).
36. Z. Wen, Z. Mai, X. Zhu, T. Wu, Y. Chen, D. Geng, J. Wang, Mesenchymal stem cell-derived exosomes ameliorate cardiomyocyte apoptosis in hypoxic conditions through microRNA144 by targeting the PTEN/AKT pathway. *Stem Cell Res. Ther.* **11**, 36 (2020).
37. M. Piffoux, A. K. A. Silva, C. Wilhelm, F. Gazeau, D. Tareste, Modification of extracellular vesicles by fusion with liposomes for the design of personalized biogenic drug delivery systems. *ACS Nano* **12**, 6830–6842 (2018).
38. Y. Lin, J. Wu, W. Gu, Y. Huang, Z. Tong, L. Huang, J. Tan, Exosome–liposome hybrid nanoparticles deliver CRISPR/Cas9 system in MSCs. *Adv. Sci.* **5**, 1700611 (2018).
39. K. B. Knudsen, H. Northeved, E. K. Pramod Kumar, A. Permin, T. Gjetting, T. L. Andresen, S. Larsen, K. M. Wegener, J. Lykkesfeldt, K. Jantzen, S. Loft, P. Møller, M. Roursgaard, In vivo toxicity of cationic micelles and liposomes. *Nanomedicine* **11**, 467–477 (2015).
40. J. Kiskis, I. Horvath, P. Wittung-Stafshede, S. Rocha, Unraveling amyloid formation paths of Parkinson's disease protein α-synuclein triggered by anionic vesicles. *Q. Rev. Biophys.* **50**, e3 (2017).
41. T. S. Choi, J. Y. Han, C. E. Heo, S. W. Lee, H. I. Kim, Electrostatic and hydrophobic interactions of lipid-associated α-synuclein: The role of a water-limited interfaces in amyloid fibrillation. *Biochim. Biophys. Acta* **1860**, 1854–1862 (2018).
42. V. Shah, O. Taratula, O. B. Garbuzenko, M. L. Patil, R. Savla, M. Zhang, T. Minko, Genotoxicity of different nanocarriers: Possible modifications for the delivery of nucleic acids. *Curr. Drug Discov. Technol.* **10**, 8–15 (2013).
43. C. Spuch, C. Navarro, Liposomes for targeted delivery of active agents against neurodegenerative diseases (Alzheimer's disease and Parkinson's disease). *J. Drug Deliv.* **2011**, 469679 (2011).
44. R. P. Araldi, F. D'amelio, H. Vigerelli, T. C. de Melo, I. Kerkis, Stem cell-derived exosomes as therapeutic approach for neurodegenerative disorders: From biology to biotechnology. 9, 2663 (2020).
45. Y. T. Sato, K. Umezaki, S. Sawada, S. A. Mukai, Y. Sasaki, N. Harada, H. Shiku, K. Akiyoshi, Engineering hybrid exosomes by membrane fusion with liposomes. *Sci. Rep.* **6**, 21933 (2016).
46. L. Li, D. He, Q. Guo, Z. Zhang, D. Ru, L. Wang, K. Gong, F. Liu, Y. Duan, H. Li, Exosome-liposome hybrid nanoparticle codelivery of TP and miR497 conspicuously overcomes chemoresistant ovarian cancer. *J. Nanobiotechnology* **20**, 50 (2022).
47. M. Zhu, S. Rajamani, J. Kaylor, S. Han, F. Zhou, A. L. Fink, The flavonoid baicalein inhibits fibrillation of α-synuclein and disaggregates existing fibrils. *J. Biol. Chem.* **279**, 26846–26857 (2004).
48. E. Paleček, J. Tkáč, M. Bartošík, T. Bertók, V. Ostatná, J. Paleček, Electrochemistry of nonconjugated proteins and glycoproteins. Toward sensors for biomedicine and glycomics. *Chem. Rev.* **115**, 2045–2108 (2015).
49. L. Palazzi, E. Bruzzone, G. Bisello, M. Leri, M. Stefani, M. Bucciantini, P. P. De Laureto, Oleuropein aglycone stabilizes the monomeric α-synuclein and favours the growth of non-toxic aggregates. *Sci. Rep.* **8**, 8337 (2018).
50. P. Borah, A. Sanjeev, V. S. K. Mattaparthi, Computational investigation on the effect of Oleuropein aglycone on the α-synuclein aggregation. *J. Biomol. Struct. Dyn.* **39**, 1259–1270 (2021).
51. B. I. Giasson, I. V. J. Murray, J. Q. Trojanowski, V. M.-Y. Lee, A hydrophobic stretch of 12 amino acid residues in the middle of α-synuclein is essential for filament assembly. *J. Biol. Chem.* **276**, 2380–2386 (2001).
52. S. Mehra, L. Gadhe, R. Bera, A. S. Sawner, S. K. Maji, Structural and functional insights into α-synuclein fibril polymorphism. *Biomolecules* **11**, 1419 (2021).
53. E. A. Waxman, J. R. Mazzulli, B. I. Giasson, Characterization of hydrophobic residue requirements for α-synuclein fibrillization. *Biochemistry* **48**, 9427–9436 (2009).
54. Y. Jin, F. Li, B. Sonoustoun, N. C. Kondru, Y. A. Martens, W. Qiao, M. G. Heckman, T. C. Ikezu, Z. Li, J. D. Burgess, D. Amerna, J. O'Leary, M. A. DeTure, J. Zhao, P. J. McLean, D. W. Dickson, O. A. Ross, G. Bu, N. Zhao, APOE4 exacerbates α-synuclein seeding activity and contributes to neurotoxicity in Alzheimer's disease with Lewy body pathology. *Acta Neuropathol.* **143**, 641–662 (2022).
55. J.-Y. Shin, B. Lee, S. Ham, J. H. Kim, H. Kim, H. Kim, M. G. Jo, H. J. Kim, S. W. Park, H.-S. Kweon, Y. J. Kim, S. P. Yun, Y. Lee, Pharmacological inhibition of AIMP2 aggregation attenuates α-synuclein aggregation and toxicity in Parkinson's disease. *Biomed. Pharmacother.* **156**, 113908 (2022).
56. V. P. Torchilin, Recent advances with liposomes as pharmaceutical carriers. *Nat. Rev. Drug Discov.* **4**, 145–160 (2005).
57. H. Hourfar, F. Aliakbari, S. R. Aqdam, Z. Nayeri, H. Bardania, D. E. Otzen, D. Morshedi, The impact of α-synuclein aggregates on blood-brain barrier integrity in the presence of neurovascular unit cells. *Int. J. Biol. Macromol.* **229**, 305–320 (2023).
58. K. B. Johnsen, A. Burkhart, F. Melander, P. J. Kempen, J. B. Vejlebo, P. Siupka, M. S. Nielsen, T. L. Andresen, T. Moos, Targeting transferrin receptors at the blood-brain barrier improves the uptake of immunoliposomes and subsequent cargo transport into the brain parenchyma. *Sci. Rep.* **7**, 10396 (2017).
59. W. M. Pardridge, The blood-brain barrier: Bottleneck in brain drug development. *NeuroRx* **2**, 3–14 (2005).
60. S. M. Hernandez, E. B. Tikhonova, A. L. Karamyshev, Protein-protein interactions in α-synuclein biogenesis: New potential targets in Parkinson's disease. *Front. Aging Neurosci.* **12**, 72 (2020).
61. M. Caruana, T. Högen, J. Levin, A. Hillmer, A. Giese, N. Vassallo, Inhibition and disaggregation of α-synuclein oligomers by natural polyphenolic compounds. *FEBS Lett.* **585**, 1113–1120 (2011).

62. Y. Yao, Y. Tang, Y. Zhou, Z. Yang, G. Wei, Baicalein exhibits differential effects and mechanisms towards disruption of α-synuclein fibrils with different polymorphs. *Int. J. Biol. Macromol.* **220**, 316–325 (2022).
63. Z. S. Marković, J. M. Dimitrić Marković, D. Milenković, N. Filipović, Mechanistic study of the structure-activity relationship for the free radical scavenging activity of baicalein. *J. Mol. Model.* **17**, 2575–2584 (2011).
64. I. K. Lee, K. A. Kang, R. Zhang, B. J. Kim, S. S. Kang, J. W. Hyun, Mitochondria protection of baicalein against oxidative damage via induction of manganese superoxide dismutase. *Environ. Toxicol. Pharmacol.* **31**, 233–241 (2011).
65. K. A. Kang, R. Zhang, M. J. Piao, S. Chae, H. S. Kim, J. H. Park, K. S. Jung, J. W. Hyun, Baicalein inhibits oxidative stress-induced cellular damage via antioxidant effects. *Toxicol. Ind. Health* **28**, 412–421 (2012).
66. A. A. Khalil, M. M. Rahman, A. Rauf, M. R. Islam, S. J. Manna, A. A. Khan, S. Ullah, M. N. Akhtar, A. S. M. Aljohani, W. Al Abdulmonem, J. Simal-Gandara, Oleuropein: Chemistry, extraction techniques and nutraceutical perspectives—An update. *Crit. Rev. Food Sci. Nutr.* , 1–22 (2023).
67. R. Zhang, X. Qin, F. Kong, P. Chen, G. Pan, Improving cellular uptake of therapeutic entities through interaction with components of cell membrane. *Drug Deliv.* **26**, 328–342 (2019).
68. R. Daneman, A. Prat, The blood-brain barrier. *Cold Spring Harb. Perspect. Biol.* **7**, a020412 (2015).
69. A. Gonda, J. Kabagwira, G. N. Senthil, N. R. Wall, Internalization of exosomes through receptor-mediated endocytosis. *Mol. Cancer Res.* **17**, 337–347 (2019).
70. C. C. Chen, L. Liu, F. Ma, C. W. Wong, X. E. Guo, J. V. Chacko, H. P. Farhoodi, S. X. Zhang, J. Zimak, A. Ségaliny, M. Riazifar, V. Pham, M. A. Digman, E. J. Pone, W. Zhao, Elucidation of exosome migration across the blood-brain barrier model in vitro. *Cell. Mol. Bioeng.* **9**, 509–529 (2016).
71. Y. Li, B. Liu, T. Zhao, X. Quan, Y. Han, Y. Cheng, Y. Chen, X. Shen, Y. Zheng, Y. Zhao, Comparative study of extracellular vesicles derived from mesenchymal stem cells and brain endothelial cells attenuating blood-brain barrier permeability via regulating Caveolin-1-dependent ZO-1 and Claudin-5 endocytosis in acute ischemic stroke. *J. Nanobiotechnology* **21**, 70 (2023).
72. K. Marzookian, F. Aliakbari, H. Hourfar, D. E. Otzen, D. Morshedi, Secretome Derived from Umbilical cord mesenchymal stem cells exerts protective impacts on the blood-brain barrier against α-synuclein aggregates using an in vitro model. bioRxiv 2023.10.21.562544 (2023). https://doi.org/10.1101/2023.10.21.562544.
73. A. M. Morris, M. A. Watzky, J. N. Agar, R. G. Finke, Fitting neurological protein aggregation kinetic data via a 2-step, minimal/"Ockham's razor" model: The Finke-Watzky mechanism of nucleation followed by autocatalytic surface growth. *Biochemistry* **47**, 2413–2427 (2008).
74. H. Mohammad-Beigi, S. A. Shojaosadati, A. T. Marvian, J. N. Pedersen, L. H. Klausen, G. Christiansen, J. S. Pedersen, M. Dong, D. Morshedi, D. E. Otzen, Strong interactions with polyethylenimine-coated human serum albumin nanoparticles (PEI-HSA NPs) alter α-synuclein conformation and aggregation kinetics. *Nanoscale* **7**, 19627–19640 (2015).
75. O. Trott, A. J. Olson, AutoDock Vina: Improving the speed and accuracy of docking with a new scoring function, efficient optimization, and multithreading. *J. Comput. Chem.* **31**, 455–461 (2010).

Acknowledgments

Funding: This study was mainly supported by the Iran National Science Foundation (INSF), Tehran, Iran (to F.A. and D.M., grant no. 98029580), and the National Institute of Genetic Engineering and Biotechnology, Tehran, Iran (to D.M., grant no. 751). D.E.O. is grateful for support from the Lundbeck Foundation, Denmark (grant no. R276-2018- 671). **Author contributions:** Conceptualization: F.A., D.E.O., and D.M. Methodology: F.A., K.M., H.H., Z.N., N.N.B., D.E.O., and D.M. Validation: F.A., K.M., D.E.O., and D.M. Formal analysis: F.A., K.M., S.P., H.H., Z.N., A.F., N.N.B., and M.R. Investigation: F.A., K.M., S.P., H.H., Z.N., A.F., M.R., and N.N.B. Resources: D.M. Data curation: F.A., K.M., H.H., M.R., D.E.O., and D.M. Writing—original draft: F.A. Writing—review and editing: F.A., K.M., H.H., Z.N., M.R., D.E.O., and D.M. Visualization: F.A., H.H., and Z.N. Project administration: F.A. and D.M. Supervision: F.A., D.E.O., and D.M. Funding acquisition: F.A. and D.M. Software: H.H. and Z.N. **Competing interests:** The authors declare that they have no competing interests. **Data and materials availability:** All data needed to evaluate the conclusions in the paper are present in the paper and/or the Supplementary Materials.

Submitted 13 October 2023
Accepted 28 February 2024
Published 3 April 2024
10.1126/sciadv.adl3406